

# Symmetry-protected Topological Phases in Spinful Bosons with a Flat Band

Hong Yang,<sup>1</sup> Hayate Nakano,<sup>1</sup> and Hosho Katsura<sup>1,2,3</sup>

<sup>1</sup>*Department of Physics, Graduate School of Science,  
The University of Tokyo, 7-3-1 Hongo, Bunkyo-ku, Tokyo 113-0033, Japan*

<sup>2</sup>*Institute for Physics of Intelligence, The University of Tokyo,  
7-3-1 Hongo, Bunkyo-ku, Tokyo 113-0033, Japan*

<sup>3</sup>*Trans-scale Quantum Science Institute, University of Tokyo, Bunkyo-ku, Tokyo 113-0033, Japan*

(Dated: September 2, 2022)

We theoretically demonstrate that interacting symmetry-protected topological (SPT) phases can be realized with ultracold spinful bosonic atoms loaded on lattices which have a flat band at the bottom of the band structure. The SPT phases in such systems are determined by both spin and charge fluctuations at zero temperature. We find that the many-body ground states of such systems can be exactly written down in some special cases, and these exact ground states turn out to serve as representative states of the SPT phases. As a concrete example, we demonstrate that spin-1 bosons on a sawtooth chain can be in an SPT phase protected by  $\mathbb{Z}_2 \times \mathbb{Z}_2$  spin rotation symmetry or time-reversal symmetry, and this SPT phase is a result of spin fluctuations. We also show that spin-3 bosons on a kagome lattice can be in an SPT phase protected by  $D_2$  point group symmetry, and this SPT phase is however a result of charge fluctuations.

## I. INTRODUCTION

Symmetry-protected topological (SPT) phases refer to the quantum phases of those short-range entangled ground states that can never be smoothly deformed into product states while preserving certain symmetry. On the other hand, a ground state is classified into a trivial phase, if it can be smoothly deformed into a product state even when certain symmetry is imposed [1]. A product state stands for a tensor product of microscopic states and possesses no quantum entanglement, while entanglement in the SPT phases cannot be smoothly eliminated when preserving the symmetry. The Affleck-Kennedy-Lieb-Tasaki (AKLT) models provide great insight into the SPT phases of interacting bosonic systems. The AKLT models are quantum spin models that can be defined on arbitrary lattices [2, 3]. The models have exact and unique ground states, known as the valance-bond-solid (VBS) states. In a simple one dimensional (1D) chain, the spin-1 VBS state [i.e., the ground state of the spin-1 AKLT model] represents an SPT phase protected by any of the following symmetries [4–7]: (a)  $\mathbb{Z}_2 \times \mathbb{Z}_2$  spin rotation symmetry, (b) time-reversal symmetry, and (c) inversion symmetry. This SPT phase is often called the *Haldane phase*. This phase is also characterized by a nonlocal order parameter—the spin string order parameter, which quantifies the hidden antiferromagnetic order in the 1D spin-1 VBS state [5, 7–9]. In certain two and higher dimensional lattices, integer-spin VBS states can be in SPT phases if either translation symmetry or crystalline symmetry is involved, as we will discuss later.

Ultracold atoms/molecules in optical lattices serve as an ideal platform for realizing topological quantum phases due to the high tunability of interactions, the viability of building various lattice structures, and the feasibility of directly measuring nonlocal order parameters [10, 11]. Motivated by recent experimental progress, many theoretical predictions about the existence of the

Haldane phase in lattice systems of bosons [12–23] and fermions [24–32] have been made.

Alkali-metal atoms carry integer spins and are thus often treated as spinful bosons in experiments [33]. Free from the Pauli exclusion principle, one major difficulty of theoretically studying spinful boson systems lies in their immense Hilbert spaces. Therefore, except for very few rigorous results [34, 35], various approximations or constraints have been employed to simplify the problem (i.e., to reduce the Hilbert space dimension). In particular, to theoretically investigate the interacting SPT phase of bosonic atoms in 1D lattices, there have been two main approaches. One is to study the the effective spin Hamiltonians by focusing on the Mott insulating limit where the charge degree of freedom is frozen [23]. For example, the system of Mott insulating spin-1 bosons is effectively described by the bilinear-biquadratic (BLBQ) model, whose ground state has been known to exhibit the Haldane phase in a wide parameter region [36]. The other approach is to study the itinerant but spinless bosons. In the itinerant case, it is generally believed that a sufficiently strong long-range (repulsive) interaction is indispensable for triggering the SPT phase [12–20, 22]. The mechanism is as follows. At the filling of one spinless boson per site on average, if we truncate the particle number on each site to  $n = 0, 1, 2$ , one can define pseudo-spin as  $\mathcal{S}^z := n - 1$ , thus resulting in an effective spin-1 model, where the long-range repulsion acts as an anisotropic spin exchange interaction [4, 13]. However, among bosonic alkali-metal atoms, although a relatively strong dipole-dipole interaction plays the role of long-range interaction in some situations [33, 37], the dipole-dipole interaction is usually much weaker than the short-range  $s$ -wave collision, and thus the long-range interaction is negligible in many experiments [33].

In short, despite the fact that itinerant, spinful, and short-range interacting bosonic atoms are very common in experiments, 1D SPT phases (Haldane phases) in such

systems have never been investigated. What is more, to our knowledge, the study on two or higher dimensional SPT phases in systems of interacting bosonic atoms is lacking. We address these issues and argue that, when there is a flat band at the bottom of the band structure (which we dub a *bottom flat band*), with only short-range interaction, bosons with both unfrozen spin and charge degrees of freedom can be in the SPT phases.

A flat band refers to an energy band that is independent of the quasimomentum. Usually, a flat band in an optical lattice is the highest band. However, by shaking the optical lattices, one can invert the sign of hopping [38–43], and the flat band thus becomes the lowest band. Such lattice shaking techniques have been realized experimentally [44–48].

Single-body eigenstates of a flat band can usually be chosen to be strictly localized on finite lattice sites. Such eigenstates are termed as *compact localized states* (CLSs) [49, 50]. Different CLSs reside in different patches (regions) of the lattice. Short-range interaction between two bosons can only happen when their wave functions overlap. At low temperatures, bosons tend to avoid overlapping each other in order to lower the system’s energy. Let  $X$  be a  $d$ -dimensional lattice with a bottom flat band and  $N$  unit cells. When  $N$  spin- $f$  bosons are loaded on  $X$ , the wave function overlaps can be minimized if each of the  $N$  CLSs hosts a boson. In other words,  $N$  bosons are distributed into  $N$  different patches. A boson is free to move around within a patch, which gives rise to charge fluctuations in the ground state. On the other hand, since all the patches (CLSs) are occupied by bosons (i.e., the whole lattice is fully “packed” with bosons), partial overlaps between neighboring wave functions are inevitable. Nevertheless, overlaps do not always significantly raise the system’s energy: since the short-range interaction is spin-dependent, the interaction energy can still be minimized if the spins of bosons entangle in a clever way similar to a spin- $f$  VBS state. When certain parameters in the Hamiltonian are fine-tuned, the above configuration becomes the exact ground state, and the exact ground state turns out to serve as a representative state of the symmetry-protected phases of the system. (In this paper, the term “symmetry-protected phase” refers to either SPT or trivial phase.) We find that the phases are determined by the spin or charge fluctuations in the ground state.

The remaining paper is divided into two parts: Sec. II and Sec. III. In Sec. II, we use spin-1 bosons on the 1D sawtooth chain as a concrete example to demonstrate our argument. The sawtooth chain has two energy bands, and the bottom one is flat. We prove that when the interaction between spin-1 bosons is fine-tuned, the ground state is unique and can be exactly written down. The proof is based on the fact that the ground state can be exactly mapped to the 1D spin-1 VBS state. This exact ground state turns out to be in a Haldane phase protected by (a)  $\mathbb{Z}_2 \times \mathbb{Z}_2$  symmetry or (b) time-reversal symmetry, but not (c) inversion symmetry. Beyond the

fine-tuned case, based on perturbation theory and numerical calculations, we confirmed that the Haldane phase exists in a rather wide parameter region. In Sec. III, based on the results in the previous section, we discuss the SPT phases with a general setup: short-range interacting spin- $f$  bosons on a bottom-flat-band lattice  $X$  in  $d$  dimension. Let  $|\text{GS}_{f,X}\rangle$  be the many-body ground state. Let  $|\text{VBS}_{f,X'}\rangle$  be the spin- $f$  VBS state defined on a lattice  $X'$  (i.e., the ground state of the spin- $f$  AKLT model on  $X'$ ). With fine-tuned interactions,  $|\text{GS}_{f,X}\rangle$  can be exactly mapped to  $|\text{VBS}_{f,X'}\rangle$ , provided that the lattice structures of  $X$  and  $X'$  satisfy a certain relation. This proves that  $|\text{GS}_{f,X}\rangle$  is the exact and unique ground state of the itinerant spin- $f$  model. The spin fluctuations of  $|\text{GS}_{f,X}\rangle$  are inherited from  $|\text{VBS}_{f,X'}\rangle$ . Therefore, with respect to the spin rotation symmetry or the combination of spin rotation and translation symmetry, the  $d$ -dimensional symmetry-protected phase of  $|\text{GS}_{f,X}\rangle$  is identical to that of  $|\text{VBS}_{f,X'}\rangle$ . Spins in  $|\text{VBS}_{f,X'}\rangle$  are pinned to the lattice sites and cannot move. However,  $|\text{GS}_{f,X}\rangle$  is not a Mott-insulating state, i.e., spin- $f$  bosons in  $|\text{GS}_{f,X}\rangle$  have nonvanishing charge fluctuations. It turns out that in terms of crystalline symmetries (i.e., point group or space group symmetries), both spin and charge fluctuations in  $|\text{GS}_{f,X}\rangle$  together determine its symmetry-protected phase. Hence, one cannot simply conclude that the crystalline-symmetry-protected phases of  $|\text{GS}_{f,X}\rangle$  and  $|\text{VBS}_{f,X'}\rangle$  are identical, because charge fluctuations may play a nontrivial role in the former state. For example, as we will show later, interacting spin-3 bosons in the kagome lattice can be in an SPT phase protected by the point group  $D_2$  or  $D_6$ , and this SPT phase is purely a consequence of charge fluctuations at zero temperature.

## II. SPIN-1 BOSONS ON A SAWTOOTH CHAIN: AN EXAMPLE

Let us start from a simple but nontrivial model: spin-1 Bose-Hubbard model on the sawtooth chain (BHMSC). In Sec. II A, we introduce the spin-1 BHMSC and the 1D spin-1 bilinear-biquadratic (BLBQ) model. Ground state of the BLBQ model is exactly solvable at the AKLT point. In Sec. II B, we prove that in a special case where the interaction between spin-1 bosons is fine-tuned, the ground state sectors of the spin-1 BHMSC and the AKLT model can be exactly mapped to each other, which enables us to write down an exact and unique ground state of the spin-1 BHMSC. This ground state, as we will show in Sec. II C, turns out to serve as a representative state of the Haldane phase. We find that the Haldane phase in this itinerant spin-1 boson system, characterized by both nonvanishing spin and charge string order parameters, is protected by  $\mathbb{Z}_2 \times \mathbb{Z}_2$  symmetry or time-reversal symmetry. In Sec. II D, perturbation theory builds another bridge between the spin-1 BHMSC and the BLBQ model. In Sec. II E, phase diagram of the spin-1 BHMSC

is investigated by numerical calculation based on the variational uniform matrix product state (VUMPS) algorithm [51, 52], which suggests that the system can either be in gapped Haldane or gapless critical phase.

### A. Hamiltonian

For spin-1 bosons (such as  ${}^7\text{Li}$ ,  ${}^{23}\text{Na}$ ,  ${}^{39}\text{K}$ , etc.) in a lattice system, let  $\hat{a}_{r,\alpha}^\dagger$  ( $\hat{a}_{r,\alpha}$ ) be the operator that creates (annihilates) a boson at lattice site  $r$  with magnetic sublevel  $\alpha = -1, 0, 1$ . The on-site spin operator  $\hat{\mathbf{S}}_r = (\hat{S}_r^x, \hat{S}_r^y, \hat{S}_r^z)$  is defined as  $\hat{S}_r^z := \sum_{\alpha,\beta} \hat{a}_{r,\alpha}^\dagger S_{\alpha,\beta}^z \hat{a}_{r,\beta}$  with  $S_{\alpha,\beta}^z = \alpha\delta_{\alpha,\beta}$  being the  $z$ -component of the spin matrix for spin-1 (and similar definitions for  $\hat{S}_r^x$  and  $\hat{S}_r^y$ ). We also define  $\hat{n}_r := \sum_{\alpha} \hat{a}_{r,\alpha}^\dagger \hat{a}_{r,\alpha}$  which counts the particle number on site  $r$ . Spin-1 atoms in optical lattices are effectively described by the spin-1 Bose-Hubbard model [53, 54]

$$\begin{aligned} \hat{H} &= \hat{H}_{\text{hop}} + \hat{H}_{\text{int}}, \\ \hat{H}_{\text{hop}} &= - \sum_{\langle r,r' \rangle} \sum_{\alpha=-1}^1 t_{r,r'} \hat{a}_{r,\alpha}^\dagger \hat{a}_{r',\alpha} + \sum_r V_r \hat{n}_r, \\ \hat{H}_{\text{int}} &= \sum_r \left( g_{0,r} \hat{P}_r^{(0)} + g_{2,r} \hat{P}_r^{(2)} \right), \end{aligned} \quad (1)$$

where  $\hat{H}_{\text{hop}}$  is the single-body Hamiltonian which contains both hopping and on-site potential terms, and  $\hat{H}_{\text{int}}$  describes the interactions ( $s$ -wave collisions) between spin-1 bosonic atoms [33, 55]. There are two kinds of interactions:  $\hat{P}_r^{(S)}$  stands for the projection operator onto the state with total spin  $S = 0, 2$  for a pair of spin-1 bosons at site  $r$ . For example,  $\hat{P}_r^{(0)} = \hat{b}_r^\dagger \hat{b}_r$ , where

$$\hat{b}_r^\dagger := \frac{1}{\sqrt{6}} (\hat{a}_{r,0}^\dagger \hat{a}_{r,0}^\dagger - 2\hat{a}_{r,1}^\dagger \hat{a}_{r,-1}^\dagger) \quad (2)$$

creates a spin singlet.  $S = 1$  is forbidden because two spin-1 bosons on the same site never form a total spin  $S = 1$  state—such a spin state is antisymmetric. The projection operators can be explicitly expressed as  $\hat{P}_r^{(0)} = [-(\hat{\mathbf{S}}_r)^2 + (\hat{n}_r)^2 + \hat{n}_r]/6$  and  $\hat{P}_r^{(2)} = [(\hat{\mathbf{S}}_r)^2 + 2(\hat{n}_r)^2 - 4\hat{n}_r]/6$  [33, 55]. The sum of them yields the “completeness relation”:

$$\hat{P}_r^{(0)} + \hat{P}_r^{(2)} = \frac{1}{2} \hat{n}_r (\hat{n}_r - 1). \quad (3)$$

We assume the interaction strength  $g_{S,r} \geq 0$  as is the case of long-lived alkali-metal spin-1 condensates [33];  $\hat{H}_{\text{int}}$  is thus positive semidefinite.

On a sawtooth chain (see Fig. 1) with  $N$  unit cells ( $2N$  sites), the single-body Hamiltonian can be written in a compact form as [56–58]

$$\hat{H}_{\text{hop}} = \hat{H}_{\text{saw}} = \sum_{i=1}^N \sum_{\alpha=-1}^1 \hat{A}_{i,\alpha}^\dagger \hat{A}_{i,\alpha}, \quad (4)$$

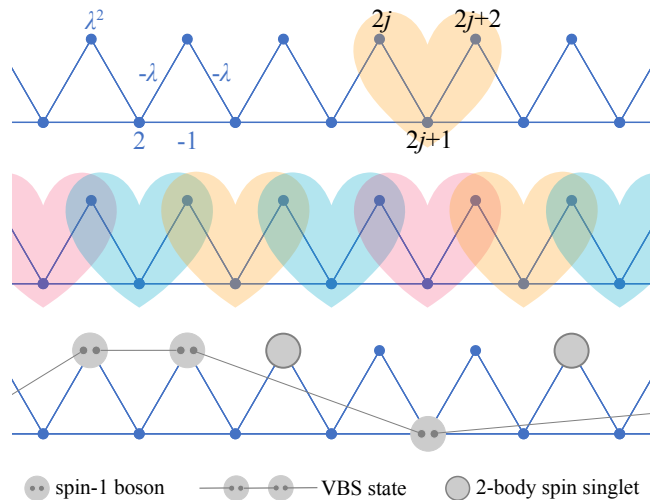


FIG. 1. (Color online) (Upper panel) The sawtooth lattice and one of its zero-energy state. The state is localized on three consecutive sites covered by the heart shape. The blue characters indicate the values of  $t_{r,r'}$  and  $V_r$ . (Middle panel) The state  $|\beta\rangle$  in Eq. (12) with a typical choice of  $\beta$ . Three different colors denote three different magnetic sublevels. Linearly independent CLSs cover the whole lattice, and two neighboring CLSs overlap on a top site. (Lower panel) The “hidden VBS order” illustrated by a typical component of  $|\text{GS}\rangle$  in Eq. (19).

where  $\hat{A}_{i,\alpha}^\dagger := \hat{a}_{2i-1,\alpha}^\dagger + \lambda \hat{a}_{2i,\alpha}^\dagger + \hat{a}_{2i+1,\alpha}^\dagger$  determines the values of  $t_{r,r'}$  and  $V_r$  in Eq. (1), and we assume  $\lambda \in \mathbb{R} \setminus \{0\}$ . Periodic boundary condition (PBC) has been imposed.  $\hat{H}_{\text{saw}}$  is positive semi-definite, and it has two energy bands: a dispersive band with energy  $\lambda^2 + 2 + 2 \cos k > 0$  and a flat band with exactly zero energy. Every eigenstate of the flat band can be chosen to be localized on three sites (see Fig. 1):

$$\hat{B}_{j,\alpha}^\dagger := \frac{1}{\sqrt{\lambda^2 + 2}} (\hat{a}_{2j,\alpha}^\dagger - \lambda \hat{a}_{2j+1,\alpha}^\dagger + \hat{a}_{2j+2,\alpha}^\dagger), \quad (5)$$

where  $\hat{B}_{j,\alpha}^\dagger$  creates a particle in a zero-energy eigenstate. In other words,  $\hat{B}_{j,\alpha}^\dagger$  is a CLS creation operator. An experimental scheme for realizing an optical sawtooth chain has been proposed [59].

Note that lattices with a bottom flat band (and CLSs) widely exist; they can actually be constructed systematically, see Sec. III B.

From now on, the total particle number on the sawtooth chain is assumed to be the same as the number of unit cells  $N$ . For simplicity, we also assume translation symmetry:  $g_{S,r} \equiv g_S^t$  for top sites ( $r = \text{even}$ ) and  $g_{S,r} \equiv g_S^b$  for bottom sites ( $r = \text{odd}$ ). The phase diagram of the spin-1 BHMSC with respect to  $(g_0^b, g_2^t, 1/\lambda)$  is shown in Fig. 2(a).

For later purposes, we also introduce the 1D spin-1 BLBQ model with PBC, whose Hamiltonian is given

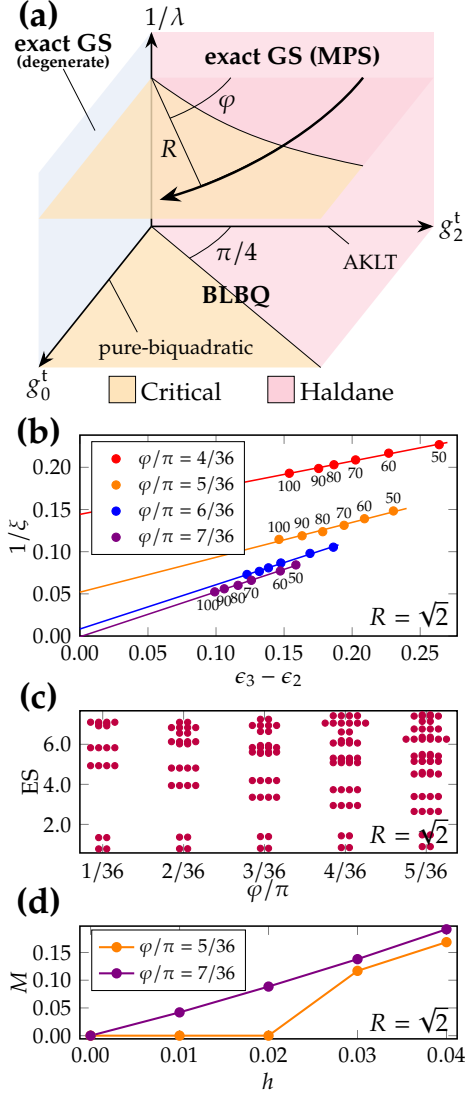


FIG. 2. (a) Schematic phase diagram of spin-1 bosons on a sawtooth chain (in the thermodynamic limit  $N \rightarrow \infty$ ) in the parameter space  $(g_0^t, g_2^t, 1/\lambda)$ . In the phase diagram we have assumed  $g_0^t, g_2^t, \lambda \geq 0$  and  $g_0^t = g_2^t = 1/\lambda^2$ . In the  $g_0^t = 0$  plane,  $\hat{H}$  has an exact and unique ground state (GS) given in Eq. (19). In the  $g_2^t = 0$  plane, the GS is massively degenerate, and the ferromagnetic states in Eq. (21) are exact ground states. Phase diagram in the  $1/\lambda \rightarrow 0$  plane, derived by perturbation theory, coincides with the phase diagram of the BLBQ model. Phase diagram in the  $1/\lambda = 1$  plane is determined by the numerical calculation based on the VUMPS algorithm. In particular, numerical results along the curved arrow parameterized by  $(\sqrt{2} \sin \varphi, \sqrt{2} \cos \varphi, 1)$  are shown in (b)–(d). (b) Scaling of the inverse correlation length  $1/\xi := \epsilon_2$  with respect to  $\epsilon_3 - \epsilon_2$ . Numbers near the data points denote the corresponding bond dimensions of each block, see Appendix E. We can see that a quantum phase transition occurs between  $\varphi = 6\pi/36$  and  $7\pi/36$ . (c) The whole entanglement spectrum (ES) in the Haldane phase region shows the even-fold degeneracy. For clarity, here we only present the lowest part of the ES. (d) Magnetization  $M$  with respect to the applied magnetic field  $h$  in  $z$ -direction. In (c) and (d), the bond dimension of each block is 50.

by [36]

$$\begin{aligned} \hat{H}_{\text{BLBQ}} &= \sum_{j=1}^N \left( \tilde{g}_0 \hat{P}_{j,j+1}^{(0)} + \tilde{g}_1 \hat{P}_{j,j+1}^{(1)} + \tilde{g}_2 \hat{P}_{j,j+1}^{(2)} \right), \\ &= J \sum_{j=1}^N \left[ \cos \theta (\hat{S}_j \cdot \hat{S}_{j+1}) + \sin \theta (\hat{S}_j \cdot \hat{S}_{j+1})^2 \right] + c, \end{aligned} \quad (6)$$

where  $\hat{P}_{j,j+1}^{(F)}$  projects the state of two neighboring sites onto the state with total spin  $F = 0, 1, 2$ , spin operators  $\{\hat{S}_j\}$  act on the spin-chain Hilbert space spanned by the  $S^z$ -basis  $\{|\psi_\alpha\rangle := |\alpha_1, \alpha_2, \dots, \alpha_N\rangle\}$ , and parameters  $(J \cos \theta, J \sin \theta, c)$  with  $J > 0$  linearly depend on  $(\tilde{g}_0, \tilde{g}_1, \tilde{g}_2)$ . This model is in the Haldane phase when  $-\pi/4 < \theta < \pi/4$ , while it is in the critical phase when  $\pi/4 \leq \theta \leq \pi/2$ . At  $\theta = \arctan(1/3)$  and  $\pi/2$ , the model is particularly known as the AKLT model and the pure-biquadratic model [60, 61], respectively. For the 1D spin-1 AKLT model

$$\hat{H}_{\text{AKLT}} = \sum_{j=1}^N \tilde{g}_2 \hat{P}_{j,j+1}^{(2)} \quad (\tilde{g}_2 > 0), \quad (7)$$

the ground state  $|\text{VBS}\rangle$  under PBC is unique and can be exactly written as a matrix product state (MPS)

$$|\text{VBS}\rangle = \sum_{\alpha_1, \dots, \alpha_N} \text{Tr}(M^{\alpha_1} M^{\alpha_2} \dots M^{\alpha_N}) |\psi_\alpha\rangle, \quad (8)$$

where  $M^{\pm 1} := \mp \sqrt{2} \sigma^{\pm}$ ,  $M^0 := \sigma^z$ , and  $\sigma^{\pm, z}$  are Pauli matrices.  $|\text{VBS}\rangle$  in Eq. (8) is known as the 1D spin-1 VBS state, which can be graphically represented as in Fig. 3(a). See Sec. III A for details.

## B. Exact ground states

Since both  $\hat{H}_{\text{saw}}$  and  $\hat{H}_{\text{int}}$  are positive semi-definite, a zero-energy ground state of  $\hat{H}$ , if exists, must satisfy (i)  $\hat{H}_{\text{saw}}|\text{GS}\rangle = 0$  and (ii)  $\hat{H}_{\text{int}}|\text{GS}\rangle = 0$ . In accordance with (i), there must be

$$|\text{GS}\rangle = \sum_{j, \mu} x_{\mathbf{n}} \left( \prod_{j=1}^N \prod_{\mu=-1}^1 (\hat{B}_{j, \mu}^\dagger)^{n_{j, \mu}} \right) |\text{vac}\rangle, \quad (9)$$

where  $x_{\mathbf{n}} \in \mathbb{C}$ ,  $\mathbf{n} = (\dots, n_{i,1}, n_{i,0}, n_{i,-1}, n_{i+1,1}, \dots)$ , and  $|\text{vac}\rangle$  is the vacuum state. Assume  $g_0^b, g_2^b > 0$ , according to Eq. (3) and the positive semidefiniteness of  $\hat{P}_r^{(S)}$ , one can conclude that

$$\begin{aligned} \text{(ii)} \iff & \left( g_0^b \hat{P}_{2j+1}^{(0)} + g_2^b \hat{P}_{2j+1}^{(2)} \right) |\text{GS}\rangle = 0, \quad \forall j \\ \iff & \hat{n}_{2j+1} (\hat{n}_{2j+1} - 1) |\text{GS}\rangle = 0, \quad \forall j \\ \iff & \hat{a}_{2j+1, \alpha} \hat{a}_{2j+1, \beta} |\text{GS}\rangle = 0, \quad \forall j, \alpha, \beta \\ \implies & x_{\mathbf{n}} = 0, \quad \forall \mathbf{n} \text{ s.t. } n_{j,1} + n_{j,0} + n_{j,-1} > 1. \end{aligned} \quad (10)$$

Equation (9) thus reduces to

$$|\text{GS}\rangle = \sum_{\boldsymbol{\beta}} y_{\boldsymbol{\beta}} |\boldsymbol{\beta}\rangle, \quad (11)$$

where  $y_{\boldsymbol{\beta}} \in \mathbb{C}$ ,  $\boldsymbol{\beta} = (\beta_1, \dots, \beta_N)$ , and

$$|\boldsymbol{\beta}\rangle := \left( \prod_{j=1}^N \hat{B}_{j,\beta_j}^\dagger \right) |\text{vac}\rangle. \quad (12)$$

A typical  $|\boldsymbol{\beta}\rangle$  is illustrated in Fig. 1. Note that  $|\boldsymbol{\beta}\rangle$ 's are linearly independent but not orthonormal because  $K_{jj'} := [\hat{B}_{j,\mu}, \hat{B}_{j',\mu}^\dagger] \neq \delta_{jj'}$ . We define the ‘‘dual operator’’ of  $\hat{B}_{j,\mu}$  as [62]

$$\hat{C}_{j,\mu} := \sum_{j'} (K^{-1})_{jj'} \hat{B}_{j',\mu} \quad (13)$$

such that  $[\hat{C}_{j,\mu}, \hat{B}_{j',\mu'}^\dagger] = \delta_{jj'} \delta_{\mu\mu'}$ . Further defining

$$\langle \tilde{\boldsymbol{\alpha}} | := \langle \text{vac} | \left( \prod_{j=1}^N \hat{C}_{j,\alpha_j} \right) \quad (14)$$

such that  $\langle \tilde{\boldsymbol{\alpha}} | \boldsymbol{\beta} \rangle = \delta_{\boldsymbol{\alpha}\boldsymbol{\beta}}$ , eigenequation  $\hat{H}|\text{GS}\rangle = 0$  then implies the matrix equation  $\sum_{\boldsymbol{\beta}} \langle \tilde{\boldsymbol{\alpha}} | \hat{H} | \boldsymbol{\beta} \rangle y_{\boldsymbol{\beta}} = 0$ . Impressively, explicit calculation shows that

$$\langle \tilde{\boldsymbol{\alpha}} | \hat{H} | \boldsymbol{\beta} \rangle = \langle \tilde{\boldsymbol{\alpha}} | \hat{H}_{\text{int}} | \boldsymbol{\beta} \rangle = \langle \psi_{\boldsymbol{\alpha}} | \hat{H}_{\text{BLBQ}} | \psi_{\boldsymbol{\beta}} \rangle, \quad (15)$$

provided that we take  $\tilde{g}_1 = 0$  and  $\tilde{g}_S = 2g_S^t d / (\lambda^2 + 2)$  in Eq. (6), where  $d > 0$  is a coefficient depending on the inverse matrix  $K^{-1}$ . Equation (15) indicates that there is a one-to-one correspondence between the zero-energy states of  $\hat{H}$  and  $\hat{H}_{\text{BLBQ}}$ . Note that such correspondence does not hold for eigenstates with nonzero energy, because  $\hat{P}_{r=\text{odd}}^{(S)} |\boldsymbol{\beta}\rangle = 0$  implies that nonzero-energy eigenstates cannot be purely spanned by  $\{|\boldsymbol{\beta}\rangle\}$ . It is known that in the following two cases,  $\hat{H}_{\text{BLBQ}}$  possesses zero-energy ground states: (1) AKLT point ( $\tilde{g}_0 = \tilde{g}_1 = 0$ ,  $\tilde{g}_2 > 0$ ) and (2) pure-biquadratic point ( $\tilde{g}_1 = \tilde{g}_2 = 0$ ,  $\tilde{g}_0 > 0$ ).

Case (1) maps to  $g_0^t = 0$  and  $g_2^t > 0$  for  $\hat{H}$ . In this case, the ground state of  $\hat{H}$  is unique, which follows from the uniqueness of the ground state of the AKLT model [2, 3]. Despite the fact that the  $|\text{GS}\rangle$  in Eq. (11) is not represented in an orthonormal basis, coefficient  $y_{\boldsymbol{\beta}}$  is identical to that of the 1D VBS state in Eq. (8):

$$y_{\boldsymbol{\beta}} = \text{Tr}(M^{\beta_1} M^{\beta_2} \dots M^{\beta_N}). \quad (16)$$

Further expanding  $\hat{B}_{j,\beta_j}^\dagger$  in terms of  $\hat{a}^\dagger$ 's, we can see that  $|\text{GS}\rangle$  is a superposition of states of the form

$$\sum_{\boldsymbol{\beta}} \text{Tr}(M^{\beta_1} M^{\beta_2} \dots M^{\beta_N}) \hat{a}_{r_1,\alpha_1}^\dagger \hat{a}_{r_2,\alpha_2}^\dagger \dots \hat{a}_{r_N,\alpha_N}^\dagger \quad (17)$$

with coefficients proportional to the power of  $-\lambda$ . In Eq. (17), we note that as long as two particles occupy the same top site, there is the identity

$$\sum_{\beta_j, \beta_{j+1}} M^{\beta_j} M^{\beta_{j+1}} \hat{a}_{\ell,\beta_j}^\dagger \hat{a}_{\ell,\beta_{j+1}}^\dagger = \sqrt{6} \hat{b}_\ell^\dagger I_2, \quad (18)$$

where  $\ell = 2j$  or  $2j+2$  and  $I_2$  is a 2-by-2 identity matrix. Equation (18) implies that Eq. (17) has ‘‘hidden VBS order’’, i.e., if we ignore all the vacant sites and sites occupied by a spin singlet, the remaining bosons form a perfect VBS state, see Fig. 1. This enables us to express  $|\text{GS}\rangle$  in an orthonormal Fock basis as

$$|\text{GS}\rangle = \sum_{\tau_1, \dots, \tau_{2N} = -1}^3 \text{Tr} \left( \prod_{j=1}^N (F^{\tau_{2j-1}} E^{\tau_{2j}}) \right) \left( \prod_{r=1}^{2N} \hat{d}_{r,\tau_r}^\dagger \right) |\text{vac}\rangle, \quad (19)$$

where  $\hat{d}_{r,\tau}^\dagger := \hat{a}_{r,\tau}^\dagger$  for  $\tau = -1, 0, 1$ , while  $\hat{d}_{r,2}^\dagger := \hat{b}_r^\dagger$  and  $\hat{d}_{r,3}^\dagger := 1$ , and

$$\begin{aligned} \sum_{\tau=-1}^3 F^\tau \hat{d}_{r,\tau}^\dagger &= \frac{1}{\sqrt{\lambda^2 + 2}} \begin{pmatrix} I_2 & -\lambda \sum_{\alpha} M^{\alpha} \hat{a}_{r,\alpha}^\dagger \\ 0 & I_2 \end{pmatrix}, \\ \sum_{\tau=-1}^3 E^\tau \hat{d}_{r,\tau}^\dagger &= \begin{pmatrix} \sum_{\alpha} M^{\alpha} \hat{a}_{r,\alpha}^\dagger & \sqrt{6} \hat{b}_r^\dagger I_2 \\ I_2 & \sum_{\alpha} M^{\alpha} \hat{a}_{r,\alpha}^\dagger \end{pmatrix}. \end{aligned} \quad (20)$$

Matrices  $F^\tau$  and  $E^\tau$  are determined from Eq. (20); the matrix product state (MPS) in Eq. (19) is injective [63]. Using Eq. (20), one can easily see that the ground state in Eq. (19) is indeed a superposition of 1D VBS states decorated with two-body singlets and/or vacant sites.

Case (2) maps to  $g_2^t = 0$  and  $g_0^t > 0$  for  $\hat{H}$ . It is obvious that the ferromagnetic states

$$\left( \sum_{r=1}^{2N} \hat{S}_r^- \right)^k \left( \prod_{j=1}^N \hat{B}_{j,1}^\dagger \right) |\text{vac}\rangle, \quad k = 0, 1, \dots, 2N \quad (21)$$

with total spin  $S_{\text{tot}} = N$  are exact ground states of  $\hat{H}$ . The spin-1 pure-biquadratic chain  $\hat{H}_{\text{PB}} = \sum_{j=1}^N \tilde{g}_0 \hat{P}_{j,j+1}^{(0)}$  (with  $\tilde{g}_0 > 0$ ) is integrable, and there are numerous states with  $S_{\text{tot}}$  ranging from 0 to  $N-1$  that are degenerate with  $(\sum_j \hat{S}_j^-)^k |\psi_{(1,1,\dots,1)}\rangle$  [60, 61, 64, 65]. The absence of ferromagnetic phase in Fig. 2(a) can thus be understood from such degeneracy: after adding interaction  $\sum_{r=\text{even}} g_2^t \hat{P}_r^{(2)}$  (with  $g_2^t > 0$ ) that disfavors the ferromagnetic states, states with smaller  $S_{\text{tot}}$  are picked up as the ground states.

### C. The Haldane phase

In this section we investigate the properties of the MPS  $|\text{GS}\rangle$ . Let  $G$  be the symmetry group of  $\hat{H}$  and  $\hat{U}(q)$  be a symmetry operation (on the Hilbert space) corresponding to the group element  $q \in G$ , i.e.,  $[\hat{H}, \hat{U}(q)] = 0$ .

Subjected to  $q$ , the unique ground state transforms as  $|\text{GS}\rangle \rightarrow \hat{U}(q)|\text{GS}\rangle$ , while the matrices in Eq. (19) transform as [66]

$$F^{\tau_{2j-1}} E^{\tau_{2j}} \rightarrow e^{i\phi_q} u_q^\dagger F^{\tau_{2j-1}} E^{\tau_{2j}} u_q, \quad (22)$$

where  $\{u_q\}_{q \in G}$  are unitary matrices which are used to classify the 1D SPT phases [4, 7, 67].

The group  $\mathbb{Z}_2 \times \mathbb{Z}_2 = \{1, \hat{U}(x), \hat{U}(y), \hat{U}(z)\}$  is a symmetry group of  $\hat{H}$ , where  $\hat{U}(\delta) := \exp(-i\pi \sum_r \hat{S}_r^\delta)$  is the spin rotation about the  $\delta = x, y, z$ -axis. The Hamiltonian is also invariant under time-reversal  $\hat{U}(\text{TR}) := \hat{U}(y)\hat{K}$  (where  $\hat{K}$  is a complex conjugation operator), space inversion  $\hat{U}(\mathcal{I})$ , combination of spin rotation and inversion  $\hat{U}(z\mathcal{I}) := \hat{U}(z)\hat{U}(\mathcal{I})$ , and combination of pseudo-spin rotation and inversion  $\hat{U}(n\mathcal{I}) := \exp[-i\pi \sum_r (\hat{n}_r - 1)]\hat{U}(\mathcal{I})$ .

For  $\hat{U}(\delta)$  and  $\hat{U}(\text{TR})$ , we can define their respective topological indices using the corresponding unitary matrices in Eq. (22) as  $\mathcal{Q}_{\mathbb{Z}_2 \times \mathbb{Z}_2} := \text{Tr}(u_x u_z u_x^\dagger u_z^\dagger)/\chi$  and  $\mathcal{Q}_{\text{TR}} := \text{Tr}(u_{\text{TR}} u_{\text{TR}}^*)/\chi$ , where  $\chi$  is the bond dimension of the MPS [68]. It is known that  $\mathcal{Q}_{\mathbb{Z}_2 \times \mathbb{Z}_2}$  equals  $-1$  for the Haldane phase protected by  $\mathbb{Z}_2 \times \mathbb{Z}_2$  symmetry while  $1$  for the trivial phase, similarly for  $\mathcal{Q}_{\text{TR}}$  [4]. When  $0 < |\lambda| < \infty$ , the system has inversion symmetry with respect to every lattice site. However, the site-centered inversion symmetry cannot protect SPT phases. The groups  $\{1, \hat{U}(\mathcal{I})\}$ ,  $\{1, \hat{U}(z\mathcal{I})\}$ , and  $\{1, \hat{U}(n\mathcal{I})\}$  can protect SPT phases only when  $\hat{U}(\mathcal{I})$  is a bond-centered inversion, see also Ref. [69] and Appendix A of Ref. [70]. When the bond-centered inversion symmetry is present, we can similarly define  $\mathcal{Q}_{\mathcal{I}} := \text{Tr}(u_{\mathcal{I}} u_{\mathcal{I}}^*)/\chi$ ,  $\mathcal{Q}_{z\mathcal{I}} := \text{Tr}(u_{z\mathcal{I}} u_{z\mathcal{I}}^*)/\chi$ , and  $\mathcal{Q}_{n\mathcal{I}} := \text{Tr}(u_{n\mathcal{I}} u_{n\mathcal{I}}^*)/\chi$ , which are quantized to  $+1$  and  $-1$  for trivial and Haldane phases, respectively [4, 5, 68]. The state  $|\text{GS}\rangle$  at  $\lambda = 0$  and  $|\lambda| \rightarrow \infty$  has bond-centered inversion symmetry. At  $|\lambda| \rightarrow \infty$ ,  $|\text{GS}\rangle$  reduces to Eq. (8). At  $\lambda = 0$ , although  $|\text{GS}_{\lambda=0}\rangle$  is not the unique ground state of  $\hat{H}|_{\lambda=0}$ , one can (in principle) always find a parent Hamiltonian that has  $|\text{GS}_{\lambda=0}\rangle$  as the unique ground state [71], and hence the state itself is still worth studying. Actually, it turns out that  $|\text{GS}_{\lambda=0}\rangle$  can be viewed as a spinful generalization of the Haldane insulator state in spinless bosons, see Appendix A. Table I summarizes the unitary matrices  $\{u_q\}$  with respect to different symmetry operations on  $|\text{GS}\rangle$ . It is then clear that the Haldane phase of  $|\text{GS}_{0 < |\lambda| < \infty}\rangle$  is protected by  $\mathbb{Z}_2 \times \mathbb{Z}_2$  symmetry or time-reversal symmetry. Interestingly, when the inversion symmetry is involved,  $|\text{GS}_{\lambda=0}\rangle$  and  $|\text{GS}_{|\lambda| \rightarrow \infty}\rangle$  can be in different phases. This difference originates from the charge fluctuations in  $|\text{GS}_{\lambda=0}\rangle$ . We claim that in general, charge fluctuations can play a nontrivial role in the SPT orders protected by crystalline symmetries, see Sec. III C for details.

Using the exact MPS in Eq. (19) and Eq. (20), various quantities that characterize the Haldane phase can be calculated analytically. For example, the spin string order parameter  $\mathcal{O}^\delta := -\lim_{L \rightarrow \infty} \lim_{N \rightarrow \infty} \frac{1}{\langle \text{GS} | \text{GS} \rangle} \langle \text{GS} | (\hat{S}_r^\delta +$

$\hat{S}_{r+1}^\delta) \exp[i\pi \sum_{k=r+2}^{r+2L-1} \hat{S}_k^\delta] (\hat{S}_{r+2L}^\delta + \hat{S}_{r+2L+1}^\delta) | \text{GS} \rangle$  and the charge string order parameter  $\mathcal{C} := -\lim_{L \rightarrow \infty} \lim_{N \rightarrow \infty} \frac{1}{\langle \text{GS} | \text{GS} \rangle} \langle \text{GS} | (\hat{n}_r + \hat{n}_{r+1} - 1) \exp\{i\pi [\sum_{k=r+2}^{r+2L-1} \hat{n}_k - (L-1)]\} (\hat{n}_{r+2L} + \hat{n}_{r+2L+1} - 1) | \text{GS} \rangle$  are found to be

$$\begin{aligned} \mathcal{O}^\delta &= \frac{16[9\lambda^6 + (5Q + 48)\lambda^2 + 3(Q + 11)\lambda^4 + 24]^2}{Q^2(3\lambda^2 + Q + 6)^2(Q + 3\lambda^2)^2}, \\ \mathcal{C} &= \frac{24(3\lambda^2 + 2)^2}{Q^2[3\lambda^4 + (Q + 12)\lambda^2 + 2(Q + 5)]}, \end{aligned} \quad (23)$$

where  $Q := \sqrt{9\lambda^4 + 36\lambda^2 + 24}$ . It can be shown that both string order parameters are nonzero:  $4/(\sqrt{6} + 3)^2 < \mathcal{O}^\delta < 4/9$  and  $0 < \mathcal{C} < 0.207$ . For open boundary condition (OBC), we can show the existence of both spin and charge edge states, see Appendix B. It is known that the (seemingly unrelated) spin string order and edge state are unified in the context of hidden  $\mathbb{Z}_2 \times \mathbb{Z}_2$  symmetry breaking. In spin chains, this can be seen by the Kennedy-Tasaki transformation [5, 7–9]. In spin- $f$  itinerant systems ( $f = \text{integer}$ ), the Kennedy-Tasaki transformation is also applicable, see Appendix C.

The “hidden VBS order” is a unique feature for the Haldane phase in systems with both spin and charge fluctuations. It is closely related to both string order parameters  $\mathcal{O}^\delta$  and  $\mathcal{C}$ . Since vacant and doubly occupied sites have zero spin, the “hidden VBS order” immediately implies the hidden antiferromagnetic order measured by  $\mathcal{O}^\delta$ . On the other hand,  $\mathcal{C}$  measures to what extent the VBS states are diluted in the background of vacant and doubly occupied sites.

In the presence of both translation symmetry and  $\mathbb{Z}_2 \times \mathbb{Z}_2$  symmetry, four distinct SPT phases can exist [72], and one of them is represented by  $|\text{GS}\rangle$ . The other three can be realized by unitary transformations of  $\hat{H}_{\text{hop}}$ , see Appendix D for details.

#### D. Perturbation theory

Beyond the cases where the ground state is exactly solvable, the phase of  $\hat{H}$  can still be determined analytically when  $|\lambda|$  is large enough. See Fig. 2(a). In the limit  $|\lambda| \rightarrow \infty$ , if we assume  $g_0^b$  and  $g_2^b$  are around the magnitude of  $\lambda^2$ , the unperturbed ground state will have each bottom site occupied by exactly one particle. In this case, perturbation theory tells us that the low-energy effective Hamiltonian of  $\hat{H}$  is given by  $\hat{H}_{\text{BLBQ}}$  in Eq. (6) with  $J \propto \lambda^{-2}$  and

$$\theta = \arctan \frac{1}{3} \cdot \frac{3g_0^t + 4g_0^t \lambda^2 / g_2^t + 2\lambda^2}{g_0^t + 2\lambda^2} \geq \arctan \frac{1}{3}, \quad (24)$$

where  $J$  and  $\theta$  are independent of  $g_S^b$ . From Eq. (24), we know that the effective model is in the Haldane phase when  $0 \leq g_0^t < g_2^t$  while in the critical phase when  $0 <$

TABLE I. Unitary matrices in Eq. (22) with respect to various symmetry operations on |GS). In accordance with the values of  $\mathcal{Q}_{\mathbb{Z}_2 \times \mathbb{Z}_2}$ ,  $\mathcal{Q}_{\text{TR}}$ ,  $\mathcal{Q}_{\mathcal{I}}$ ,  $\mathcal{Q}_{z\mathcal{I}}$ , and  $\mathcal{Q}_{n\mathcal{I}}$ , shadowed matrices denote trivial phases, while matrices without shadow denote the SPT phase. N/A means the symmetry group cannot protect the SPT phase.

	$\hat{U}(\delta)$ ( $\delta = x, y, z$ )	$\hat{U}(\text{TR})$	$\hat{U}(\mathcal{I})$	$\hat{U}(z\mathcal{I})$	$\hat{U}(n\mathcal{I})$
$\lambda = 0$	$u_\delta = \begin{pmatrix} \sigma^\delta & 0 \\ 0 & \sigma^\delta \end{pmatrix}$	$u_{\text{TR}} = \begin{pmatrix} \sigma^y & 0 \\ 0 & \sigma^y \end{pmatrix}$	$u_{\mathcal{I}} = \begin{pmatrix} 0 & -\sigma^y \\ \sigma^y & 0 \end{pmatrix}$	$u_{z\mathcal{I}} = \begin{pmatrix} 0 & -\sigma^x \\ \sigma^x & 0 \end{pmatrix}$	$u_{n\mathcal{I}} = \begin{pmatrix} 0 & \sigma^y \\ \sigma^y & 0 \end{pmatrix}$
$0 <  \lambda  < \infty$	$u_\delta = \begin{pmatrix} \sigma^\delta & 0 \\ 0 & \sigma^\delta \end{pmatrix}$	$u_{\text{TR}} = \begin{pmatrix} \sigma^y & 0 \\ 0 & \sigma^y \end{pmatrix}$	N/A	N/A	N/A
$ \lambda  \rightarrow \infty$	$u_\delta = \sigma^\delta$	$u_{\text{TR}} = \sigma^y$	$u_{\mathcal{I}} = \sigma^y$	$u_{z\mathcal{I}} = \sigma^x$	$u_{n\mathcal{I}} = \sigma^y$

$g_2^\dagger \leq g_0^\dagger$ . In particular,  $g_0^\dagger = 0$  and  $g_2^\dagger = 0$  corresponds to AKLT and pure-quadratic point, respectively.

### E. Numerical analysis

Beyond the three special planes in Fig. 2(a) where either exact ground states can be found or perturbation theory works, the phase diagram of the spin-1 BHMSC can in general be determined by numerical calculations. In the thermodynamic limit  $N \rightarrow \infty$ , we find out the phase diagram in the  $\lambda = 1$  plane in Fig. 2(a) by the VUMPS algorithm [51, 52]. Due to the fact that the total number of particles and unit cells are the same, matrices in the MPS ansatz used in the algorithm are assumed to be block-banded [73]. Besides, the maximum particle number on each site is truncated to three. See Appendix E for details of the MPS ansatz. Let  $\epsilon_i := -\ln |\lambda_i|$ , where  $\lambda_i$  is the  $i$ th largest absolute eigenvalue of the transfer matrix, and  $|\lambda_1|$  is normalized to 1. When the bond dimension  $\chi$  is extrapolated to infinity, the correlation length  $\xi := 1/\epsilon_2$  diverges for gapless phases while converges to a finite value for gapped phases. This fact is known to be well reflected in the scaling relation of  $1/\xi(\chi)$  with respect to  $\epsilon_3(\chi) - \epsilon_2(\chi)$  [74, 75], as shown in Fig. 2(b). In the region of the gapped phase in Fig. 2(a), we find that  $\mathcal{Q}_{\mathbb{Z}_2 \times \mathbb{Z}_2} = \mathcal{Q}_{\text{TR}} = -1$ , which suggests that the gapped phase is the Haldane phase. The Haldane phase is characterized by an even-fold degenerate entanglement spectrum [4], see Fig. 2(c). The ground state magnetization  $M := \lim_{N \rightarrow \infty} \langle \sum_{r=1}^{2N} \hat{S}_r^z \rangle / N$  is calculated after adding  $-h \sum_r \hat{S}_r^z$  to  $\hat{H}$ , where  $h$  is the magnetic field; see Fig. 2(d). In the gapless region,  $M$  grows almost linearly with  $h$ , which suggests that the gapless phase is the critical phase [76]. In the Haldane phase region, however,  $M$  is expected to exhibit a zero plateau for small  $h$  [76], which is indeed the case as in Fig. 2(d). Note that the phase boundary in the  $\lambda = 1$  plane is curved, see Appendix E for numerical evidence.

### F. Short summary for the spin-1 bosons on a sawtooth chain

To demonstrate how the Haldane phase emerges in short-range interacting spinful bosons loaded on lattices with a bottom flat band, we have used the spin-1 BHMSC as an example. We show that this system has some deep connections with the BLBQ model. Especially, in a special case, by an exact mapping to the ground state of the AKLT model, we obtain the exact and unique ground state of the spin-1 BHMSC. This exact ground state turns out to serve as a representative state of the Haldane phase. The Haldane phase in the spin-1 BHMSC is protected by  $\mathbb{Z}_2 \times \mathbb{Z}_2$  symmetry or time-reversal symmetry. The phase diagram of this model is obtained by perturbation theory and numerical calculations based on the VUMPS algorithm, and we find out that the Haldane phase exists in a rather wide parameter region.

## III. GENERAL THEORY

The sawtooth chain is not special in the sense that there are many other lattices possessing a bottom flat band, it is thus natural to expect that the SPT phases can be realized with spinful bosons loaded on these lattices. Our approach in the previous section can be generalized. In this section, we present a general theory on the SPT phases of spin- $f$  bosons with a bottom flat band. We first show in Sec. III A that the AKLT model and VBS state can be generalized to higher spins and higher dimensional lattices. Let  $|\text{VBS}_{f,X'}\rangle$  be the exact and unique ground state of the spin- $f$  AKLT model defined on a lattice  $X'$ . On the other hand, bottom-flat-band lattices can be constructed systematically. Let  $|\text{GS}_{f,X}\rangle$  be the ground state of  $N$  spin- $f$  bosons on a bottom-flat-band lattice  $X$  with  $N$  unit cells. In Sec. III B, we show that with fine-tuned parameters,  $|\text{GS}_{f,X}\rangle$  can be exactly mapped to  $|\text{VBS}_{f,X'}\rangle$ , provided that  $f$ ,  $X$ , and  $X'$  satisfy a certain relation. This means that  $|\text{GS}_{f,X}\rangle$  is the exact and unique ground state of the itinerant spin- $f$  model. In Sec. III C, with various  $f$  and  $X$ , we classify the quantum phases of  $|\text{GS}_{f,X}\rangle$ 's from the viewpoint of SPT orders. In particular, we find that in terms of crystalline symmetries, not only spin fluctuations but also charge fluc-

tuations in  $|\text{GS}_{f,X}\rangle$  determines the symmetry-protected phase. Although our analysis in Sec. III C is based on the exact ground states (as a consequence of fine-tuned parameters), it is expected that the SPT phases can be found in rather wide parameter regions, like the case in the spin-1 BHMSC.

### A. Generalized AKLT models and VBS states

It is known that VBS states can be constructed on any lattice in any dimensions [3, 77, 78]. In this article, we only consider bosonic spin- $f$  VBS states ( $f = \text{integer}$ ). Let  $X' = (\Lambda_{X'}, \mathcal{B}_{X'})$  be a lattice (graph) where  $\Lambda_{X'}$  is the set of sites (vertices) and  $\mathcal{B}_{X'}$  is the set of bonds (edges). A bond is defined by two sites  $\{\mathbf{j}, \mathbf{j}'\}$  with  $\mathbf{j}, \mathbf{j}' \in \Lambda_{X'}$ . We assume that every site in  $X'$  is directly connected to  $2f$  other sites, i.e.,  $|\{\mathbf{j}' \in \Lambda_{X'} | \{\mathbf{j}, \mathbf{j}'\} \in \mathcal{B}_{X'}\}| = 2f, \forall \mathbf{j}$ . (In other words,  $X'$  is a regular graph of degree  $2f$ .) When there is a spin- $f$  degree of freedom residing in every site of  $X'$ , an AKLT-type quantum spin model can be defined on  $X'$  as

$$\hat{H}_{\text{AKLT}}^{f,X'} := \tilde{g}_{2f} \sum_{\{\mathbf{j}, \mathbf{j}'\} \in \mathcal{B}_{X'}} \hat{P}_{\mathbf{j}, \mathbf{j}'}^{(2f)} \quad (\tilde{g}_{2f} > 0), \quad (25)$$

where the operator  $\hat{P}_{\mathbf{j}, \mathbf{j}'}^{(2f)}$  projects the state of two spin- $f$ 's on two sites  $\mathbf{j}, \mathbf{j}'$  onto the state with total spin  $2f$ .

It has been proved that when  $|\Lambda_{X'}| = N < \infty$ ,  $\hat{H}_{\text{AKLT}}^{f,X'}$  has an exact and unique ground state [7, 79], known as a VBS state:

$$|\text{VBS}_{f,X'}\rangle = \sum_{\alpha_1, \dots, \alpha_N = -f}^f S_{\alpha_1, \dots, \alpha_N} |\psi_{\alpha_1, \dots, \alpha_N}\rangle, \quad (26)$$

where  $\{|\psi_{\alpha_1, \alpha_2, \dots, \alpha_N}\rangle\}$  is the spin  $S^z$ -basis and the coefficient  $S_{\alpha_1, \dots, \alpha_N}$  encodes short-range entanglement between the spins. When  $X'$  is the simple 1D linear chain with  $f = 1$ ,  $\hat{H}_{\text{AKLT}}^{f,X'}$  reduces to Eq. (7), and its ground state is the 1D spin-1 VBS state in Eq. (8), and  $S_{\alpha_1, \dots, \alpha_N} = y_{\alpha}$  in Eq. (16). Structure of this VBS state can be understood as follows: as shown in Fig. 3(a), each spin-1 is viewed as a composite state of two spin-1/2's, and a pair of spin-1/2's on two neighboring sites forms a spin singlet. For  $\hat{H}_{\text{AKLT}}^{f,X'}$  on a general  $X'$ , the ground state  $|\text{VBS}_{f,X'}\rangle$  can be constructed in the same manner: each spin- $f$  is regarded as a composite state of  $2f$  spin-1/2's, and a singlet is formed between two spin-1/2's in every bond  $\{\mathbf{j}, \mathbf{j}'\} \in \mathcal{B}_{X'}$  [3, 77]. Some other graph representations of VBS states in 2D and 3D are given in Fig. 3(b)-(d).

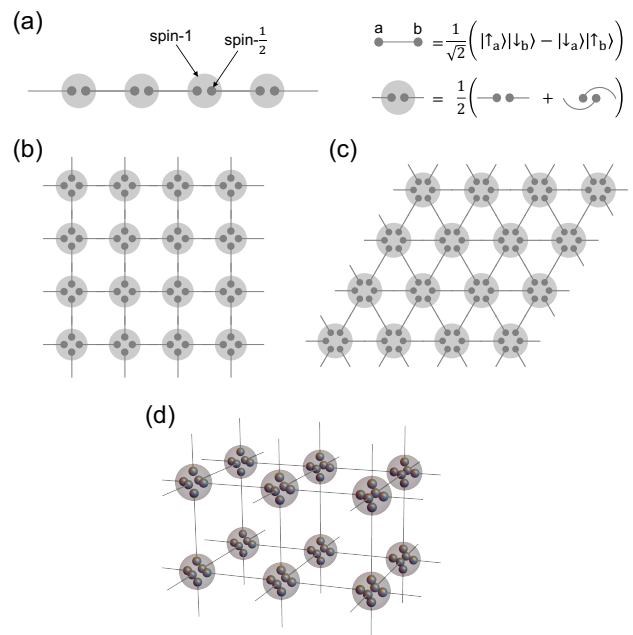


FIG. 3. Examples of bosonic VBS states. Each spin- $f$  is regarded as a composite state of  $2f$  spin-1/2's, and a spin singlet is formed between two spin-1/2's on neighboring sites. (a) 1D spin-1 VBS state, whose expression is given in Eq. (8). (b) 2D spin-2 VBS state on a square lattice. (c) 2D spin-3 VBS state on a triangular lattice. (d) 3D spin-3 VBS state on a cubic lattice.

### B. Ground states of spin- $f$ bosons with a bottom flat band

Many kinds of atoms carry integer spins, among which alkali-metal atoms are often used in experiments [33]. Alkali-metal atoms have two hyperfine levels, and each level carries integer spin  $f$ , see Table II. Due to the hyperfine interaction, the level with smaller  $f$  has lower energy. Therefore, alkali-metal atoms stay in lower hyperfine level when they are optically trapped without external pumping. For example, as shown in Table II,  $^{85}\text{Rb}$  atoms are usually regarded as spin-2 bosons, while they can in principle be spin-3 bosons if one can pump them into the  $f = 3$  hyperfine state.

atom	$f$
$^1\text{H}$	0, 1
$^7\text{Li}$ , $^{23}\text{Na}$ , $^{39}\text{K}$ , $^{41}\text{K}$ , $^{87}\text{Rb}$	1, 2
$^{85}\text{Rb}$	2, 3
$^{133}\text{Cs}$	3, 4

TABLE II. Some alkali-metal atoms and their hyperfine spins  $f$  [33].

We have seen that the single-particle CLSs play a crucial role in the nontrivial many-body ground state. The CLSs exist not only in the sawtooth chain but also

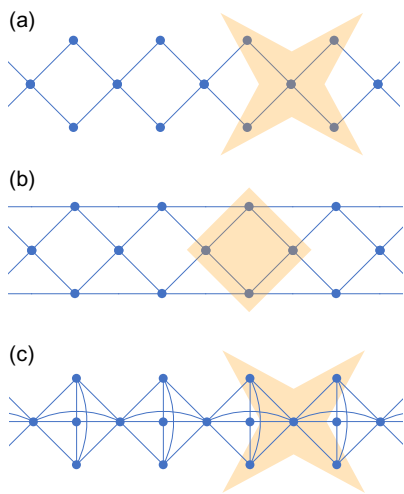


FIG. 4. Other examples of 1D lattices that can be used to construct nontrivial ground states with spin-1 bosons. Allowed hopping process between two sites is illustrated by a bond. (a) Diamond chain. A  $\pi$  flux threads each plaquette [88]. A CLS covers five sites, as denoted by the four-pointed star. (b) Kagome ladder, an example of the line graph construction [78, 81]. A CLS is denoted by the square. (c) Pyramid chain, an example of the cell construction [7]. A CLS is denoted by the four-pointed star.

in all the finite-range hopping lattices possessing a flat band [49, 50]. In fact, there are various systematic approaches to construct flat-band lattices [7, 49, 56, 57, 80–86], among which Tasaki’s cell construction [56, 57] and Mielke’s line graph construction [80–82] always yields a bottom flat band [87]. These systematic constructions generate infinitely many lattices in  $d \geq 1$  dimensions, such as those shown in Fig. 4 for  $d = 1$  and Fig. 5 for  $d = 2, 3$ .

Let  $X = (\Lambda_X, \mathcal{B}_X)$  be a bottom-flat-band lattice where  $\Lambda_X$  is the set of sites and  $\mathcal{B}_X$  is the set of bonds. A bond is defined by two sites  $\{\mathbf{r}, \mathbf{r}'\}$  with  $\mathbf{r}, \mathbf{r}' \in \Lambda_X$ . Let  $\hat{H}_{\text{hop}}^{f,X}$  be a single-body Hamiltonian for spin- $f$  bosons on  $X$ :

$$\hat{H}_{\text{hop}}^{f,X} = - \sum_{\{\mathbf{r}, \mathbf{r}'\} \in \mathcal{B}_X} \sum_{\alpha=-f}^f t_{\mathbf{r}, \mathbf{r}'} \hat{a}_{\mathbf{r}, \alpha}^\dagger \hat{a}_{\mathbf{r}', \alpha} + \sum_{\mathbf{r} \in \Lambda_X} V_{\mathbf{r}} \hat{n}_{\mathbf{r}}, \quad (27)$$

where  $\hat{a}_{\mathbf{r}, \alpha}^\dagger$  creates a boson with magnetic sublevel  $\alpha$  at site  $\mathbf{r}$ . Let  $N$  be the total number of unit cells in  $X$ . The assumption that  $X$  has a bottom flat band means that the single-particle ground state degeneracy of  $\hat{H}_{\text{hop}}^{f,X}$  is  $N(2f + 1)$ . The corresponding CLSs are localized on  $N$  different positions and are related to each other by lattice translation vectors [90]. Shapes of some CLSs are shown in Fig. 4 and 5. Let  $(\hat{B}_{j,\alpha}^{f,X})^\dagger$  be the creation operator of a CLS, where  $j = 1, 2, \dots, N$  labels different positions. A fully packed state (FPS) on  $X$  is defined as a product of  $N$  CLSs:  $(\hat{B}_{1,\alpha_1}^{f,X})^\dagger (\hat{B}_{2,\alpha_2}^{f,X})^\dagger \dots (\hat{B}_{N,\alpha_N}^{f,X})^\dagger |\text{vac}\rangle$ . In an FPS, the lattice is “fully packed” by  $N$  particles. For example,

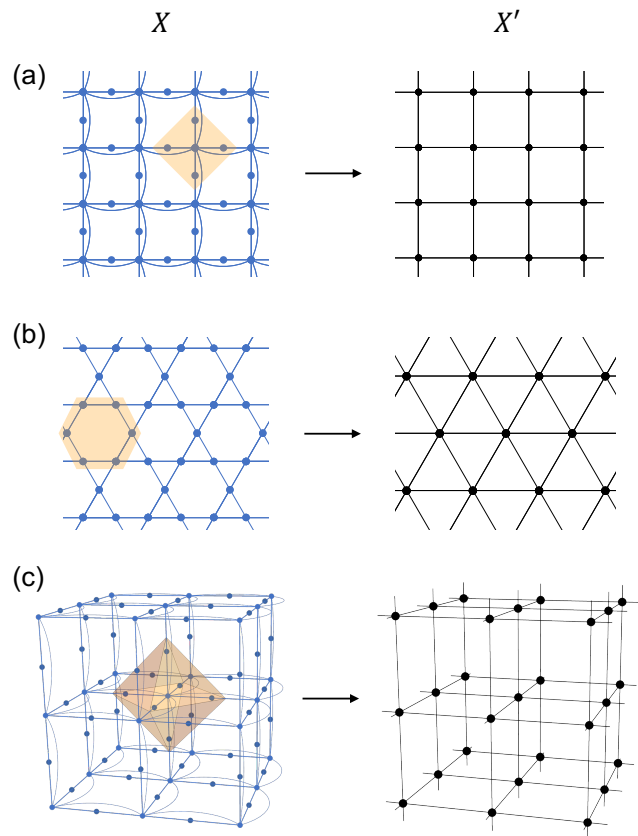


FIG. 5. Examples of higher dimensional lattices  $X$  with a bottom flat band (left column) and their corresponding lattices  $X'$  where the AKLT models are defined (right column). In  $X$ , allowed hopping processes are illustrated by bonds. In  $X'$ , a bond represents interaction between two spins. (a) 2D Tasaki lattice (left), an example of the cell construction [56, 57]. A CLS is localized on five sites, as pictured by the square. All the CLSs are related each other by lattice translation vectors. Every CLS overlaps with 4 other CLSs, thus  $f$  should be  $4/2 = 2$ . The corresponding AKLT model lives on a square lattice (right). (b) Kagome lattice (left), an example of the line graph construction [81]. A CLS is localized on a hexagon. Every CLS overlaps with  $2f = 6$  other CLSs, and the corresponding AKLT model lives on a triangular lattice (right). An optical kagome lattice has been realized experimentally [89]. (c) 3D Tasaki lattice (left), another example of the cell construction [56, 57]. A CLS is localized on seven sites, as covered by the octahedron. Every CLS overlaps with  $2f = 6$  other CLSs, the corresponding AKLT model thus lives on a cubic lattice (right).

$|\beta\rangle$  in Eq. (12) is an FPS in the sawtooth chain.

We now consider another lattice  $X' = (\Lambda_{X'}, \mathcal{B}_{X'})$  with  $|\Lambda_{X'}| = N$ , and each site  $\mathbf{j} \in \Lambda_{X'}$  represents a CLS in the FPS of  $X$ . Two sites in  $X'$  are directly connected iff the two corresponding CLSs in the FPS (partially) overlap. For example, as shown in Fig. 5, if  $X$  is the 2D (3D) Tasaki lattice,  $X'$  will be the square (cubic) lattice, while if  $X$  is the kagome lattice,  $X'$  will then be the triangular lattice. In the following, we require that  $f$  and

$X$  are chosen such that  $X'$  satisfies the condition  $|\{j' \in \Lambda_{X'} | \{j, j'\} \in \mathcal{B}_{X'}\}| = 2f, \forall j \in \Lambda_{X'}$ . Define  $\Lambda_X^{[k]} \subset \Lambda_X$  as a set of sites where  $k$  CLSs in the FPS overlap. For example, in the sawtooth chain  $\Lambda_X = \Lambda_X^{[1]} \cup \Lambda_X^{[2]}$ , where  $\Lambda_X^{[1]}$  is the set of all the bottom sites and  $\Lambda_X^{[2]}$  is all the top sites. We further require that every site  $\mathbf{r} \in \Lambda_X$  is shared by no more than two CLSs in the FPS, i.e.,  $\Lambda_X^{[k]} = \emptyset$  for  $k > 2$ . We then define the spin model  $\hat{H}_{\text{AKLT}}^{f, X'}$  on  $X'$ , as introduced in Sec. III A.

The  $s$ -wave interaction between two spin- $f$  bosons at position  $\mathbf{r}$  is given by  $\sum_{S=0,2,\dots,2f} g_{S,\mathbf{r}} \hat{P}_{\mathbf{r}}^{(S)}$ , where the  $\text{SO}(3)$ -invariant operator  $\hat{P}_{\mathbf{r}}^{(S)}$  projects the state onto total spin  $S = \text{even}$  and satisfies the “completeness relation”  $\sum_S \hat{P}_{\mathbf{r}}^{(S)} = \hat{n}_{\mathbf{r}}(\hat{n}_{\mathbf{r}} - 1)/2$  [33]. (For interaction between alkali-metal atoms, it is sufficient to consider the short-range  $s$ -wave scattering [33].) Spin- $f$  bosons in optical lattices are described by the spin- $f$  Bose-Hubbard model. On the lattice  $X$ , the model is given by

$$\begin{aligned} \hat{H}^{f,X} &:= \hat{H}_{\text{hop}}^{f,X} + \hat{H}_{\text{int}}^{f,X}, \\ \hat{H}_{\text{int}}^{f,X} &:= \sum_{\mathbf{r} \in \Lambda_X} \sum_{S=0,2,\dots,2f} g_{S,\mathbf{r}} \hat{P}_{\mathbf{r}}^{(S)}. \end{aligned} \quad (28)$$

If  $N$  spin- $f$  bosons are loaded on  $X$  and  $g_{2f,\mathbf{r}} > 0$  and  $g_{S<2f,\mathbf{r}} = 0$  for all  $\mathbf{r} \in \Lambda_X^{[2]}$ , following Sec. II B, the zero-energy ground states of  $\hat{H}^{f,X}$  in Eq. (28) and  $\hat{H}_{\text{AKLT}}^{f, X'}$  in Eq. (25) can thus be exactly mapped to each other, just as Eq. (15). See Appendix F for discussions on the uniqueness of the ground state of  $\hat{H}^{f,X}$ .

Let us see some concrete examples. In  $d = 1$  dimension, besides the sawtooth chain, spin-1 bosons can be loaded on the lattices in Fig. 4 as well. In  $d = 2$ , the 2D Tasaki lattice matches spin-2 bosons, and the corresponding spin-2 AKLT model lives on a square lattice with the VBS ground state in Fig. 3(b). The kagome lattice is suitable for spin-3 bosons, while the corresponding AKLT model has the spin-3 VBS ground state on a triangular lattice as shown Fig. 3(c). On the other hand, spin-3 bosons are also compatible with the 3D Tasaki lattice, which corresponds to a 3D spin-3 VBS state in Fig. 3(d). In fact, the Tasaki lattice can be constructed in any dimension, and the sawtooth chain can actually be regarded as the 1D Tasaki lattice [56, 57]. In general, the  $d$ -dimensional Tasaki lattice matches spin- $d$  bosons, and the corresponding AKLT model lives on a  $d$ -dimensional hypercubic lattice.

Let  $|\text{GS}_{f,X}\rangle$  be the exact and unique ground state of  $\hat{H}^{f,X}$ . In terms of the Fock basis,  $|\text{GS}_{f,X}\rangle$  reads

$$\begin{aligned} |\text{GS}_{f,X}\rangle &= \sum_{\alpha_1, \dots, \alpha_N = -f}^f S_{\alpha_1, \dots, \alpha_N} \sum_{\mathbf{r}_1, \dots, \mathbf{r}_N} C_{\mathbf{r}_1, \dots, \mathbf{r}_N} \\ &\times \hat{a}_{\mathbf{r}_1, \alpha_1}^\dagger \dots \hat{a}_{\mathbf{r}_N, \alpha_N}^\dagger |\text{vac}\rangle, \end{aligned} \quad (29)$$

where  $S_{\alpha_1, \dots, \alpha_N}$  and  $C_{\mathbf{r}_1, \dots, \mathbf{r}_N}$  are coefficients that correspond to different spin and charge configurations, respec-

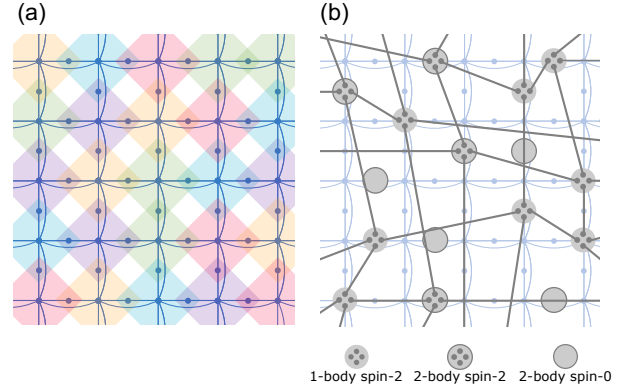


FIG. 6. Components of the exact ground state of spin-2 bosons on the 2D Tasaki lattice. (a) Visualization of Eq. (30) with a typical choice of  $\alpha_1, \dots, \alpha_N$ . The five possible values of  $\alpha_j$  are represented by five different colors. Equation (30) is a fully packed state (FPS). (b) Visualization of Eq. (31) with a typical choice of  $\mathbf{r}_1, \dots, \mathbf{r}_N$ . The state exhibits “hidden VBS order”: if we ignore all 2-body spin singlets, the remaining particles form a VBS state. The ground state can be viewed as a linear combination of such states with different charge configurations.

tively. Summing over the charge degrees of freedom first gives a FPS:

$$\begin{aligned} &\sum_{\mathbf{r}_1, \dots, \mathbf{r}_N} C_{\mathbf{r}_1, \dots, \mathbf{r}_N} \hat{a}_{\mathbf{r}_1, \alpha_1}^\dagger \dots \hat{a}_{\mathbf{r}_N, \alpha_N}^\dagger |\text{vac}\rangle \\ &= (\hat{B}_{1, \alpha_1}^{f,X})^\dagger (\hat{B}_{2, \alpha_2}^{f,X})^\dagger \dots (\hat{B}_{N, \alpha_N}^{f,X})^\dagger |\text{vac}\rangle. \end{aligned} \quad (30)$$

$|\text{GS}_{f,X}\rangle$  is a linear combination of FPSs with different spin configurations, and the coefficients  $S_{\alpha_1, \dots, \alpha_N}$  in Eq. (29) and Eq. (26) are identical. However, if we sum over the spin degrees of freedom first:

$$\sum_{\alpha_1, \dots, \alpha_N = -f}^f S_{\alpha_1, \dots, \alpha_N} \hat{a}_{\mathbf{r}_1, \alpha_1}^\dagger \dots \hat{a}_{\mathbf{r}_N, \alpha_N}^\dagger |\text{vac}\rangle, \quad (31)$$

we will get a state with “hidden VBS order”.  $|\text{GS}_{f,X}\rangle$  can then be alternatively viewed as a linear combination of such states with different charge configurations. The above analysis suggests that the FPS and “hidden VBS order” are two different but equivalent pictures of understanding the structure of the ground states, and they together reflect spin and charge fluctuations at zero temperature. Figure 6 gives examples of an FPS and a state with “hidden VBS order” of spin-2 bosons on the 2D Tasaki lattice.

Let us note that although an exact ground state  $|\text{GS}_{f,X}\rangle$  is a result of fine-tuned interactions, one can readily believe that quantum phase represented by  $|\text{GS}_{f,X}\rangle$  (to be discussed in Sec. III C) exists in rather wide parameter regions, as supported by the evidences shown in Sec. II D and II E for the sawtooth chain.

### C. Classifying the ground states from the viewpoint of SPT phases

As the unique ground state,  $|\text{GS}_{f,X}\rangle$  preserves all the symmetries of the system. One can always think of  $|\text{GS}_{f,X}\rangle$  as a representative state of a certain disordered, gapped, short-range entangled, and symmetry-protected quantum phase. In order to classify the phases represented by  $|\text{GS}_{f,X}\rangle$  with various  $f$  and  $X$ , there are two main questions that we need to answer. First, what is the phase of the corresponding VBS state  $|\text{VBS}_{f,X'}\rangle$ ? Second, are the two states  $|\text{GS}_{f,X}\rangle$  and  $|\text{VBS}_{f,X'}\rangle$  in exactly the same phase?

Recall that for  $f = 1$  and  $X$  being the sawtooth chain, the answers to the two questions have been completely listed in Table I. The two states Eq. (19) and Eq. (8) are in the same phase except when the inversion symmetry is involved. In  $d > 1$  dimensions, however, regarding the first question, given an arbitrary  $f$  and  $X'$ , there is so far no complete answer about the phase of  $|\text{VBS}_{f,X'}\rangle$  in terms of all of its symmetry groups. Nevertheless, it has been known that with on-site symmetry [91] only,  $|\text{VBS}_{f,X'}\rangle$  always represents a trivial phase in  $d > 1$ , while the combination of on-site symmetry and translation symmetry can give an SPT/trivial classification [92]. In addition, we show later that crystalline symmetries alone can also give an SPT/trivial classification for  $|\text{VBS}_{f,X'}\rangle$ . Regarding the second question, we claim that  $|\text{GS}_{f,X}\rangle$  and  $|\text{VBS}_{f,X'}\rangle$  are always in the same phase protected by on-site symmetry alone or the combination of on-site and translation symmetry. However, their phases should be investigated on a case-by-case basis when crystalline symmetries come into play. In particular, we find that the charge fluctuations in  $|\text{GS}_{f,X}\rangle$  can play a nontrivial role in the SPT orders protected by crystalline symmetries. In the following, for simplicity, we only focus on  $d = 2$  systems with  $f = 2, 3$ . The analysis however applies to general cases.

In terms of the combination of  $\text{SO}(3)$  spin rotation and translation symmetry [denote the symmetry group as  $\text{SO}(3) \times \text{trn}$ ], the spin-2 VBS state on a square lattice  $|\text{VBS}_{2,\square}\rangle$  is in an SPT phase [1, 93, 94], while the spin-3 VBS state on a triangular lattice  $|\text{VBS}_{3,\triangle}\rangle$  represents a trivial phase [95]. A key observation is that  $|\text{GS}_{f,X}\rangle$  can always be smoothly deformed to  $|\text{VBS}_{f,X'}\rangle$  without breaking the  $\text{SO}(3) \times \text{trn}$  symmetry, such that the two states are in the same phase. For example, let  $\hat{B}_{1,\alpha}^{3,\star}$  be one of the CLS operators on the kagome lattice, whose exact form is given by

$$\hat{B}_{1,\alpha}^{3,\star} = \frac{1}{\sqrt{6}} \sum_{x=1}^6 (-1)^x \hat{a}_{x,\alpha}, \quad (32)$$

where the six sites labeled by  $x$  form vertices of a hexagon, as shown in Fig. 7. We then define a  $\lambda$ -deformed

CLS operator as

$$\hat{B}_{1,\alpha}^{3,\star}(\lambda) = \frac{1}{\sqrt{\lambda^2 + 5}} \left( \sum_{x=1}^6 (-1)^x \hat{a}_{x,\alpha} + \lambda \hat{a}_{6,\alpha} \right), \quad (33)$$

which satisfies  $\hat{B}_{1,\alpha}^{3,\star}(1) = \hat{B}_{1,\alpha}^{3,\star}$  and  $\lim_{\lambda \rightarrow \infty} \hat{B}_{1,\alpha}^{3,\star}(\lambda) = \hat{a}_{6,\alpha}$ . By applying lattice translation vectors, we can get all the other  $\hat{B}_{j,\alpha}^{3,\star}(\lambda)$  with  $j = 2, \dots, N$ . Now consider the state defined on the kagome lattice

$$|\text{GS}_{3,\star}(\lambda)\rangle = \sum_{\alpha_1, \dots, \alpha_N = -3}^3 S_{\alpha_1, \dots, \alpha_N} \prod_{j=1}^N \left( \hat{B}_{j,\alpha_j}^{3,\star}(\lambda) \right)^\dagger |\text{vac}\rangle, \quad (34)$$

where  $\{S_{\alpha_1, \dots, \alpha_N}\}$  are chosen such that  $|\text{GS}_{3,\star}(1)\rangle = |\text{GS}_{3,\star}\rangle$  is the original ground state of  $\hat{H}^{3,\star}$ . One can then easily see that  $\lim_{\lambda \rightarrow \infty} |\text{GS}_{3,\star}(\lambda)\rangle = |\text{VBS}_{3,\triangle}\rangle$  and the state  $|\text{GS}_{3,\star}(\lambda)\rangle$  remains  $\text{SO}(3) \times \text{trn}$  symmetric and short-range entangled for  $1 < \lambda < \infty$ . Therefore,  $|\text{GS}_{3,\star}\rangle$  and  $|\text{VBS}_{3,\triangle}\rangle$  are smoothly connected and in the same trivial phase protected by  $\text{SO}(3) \times \text{trn}$ . For an arbitrary  $f$  and  $X$ , a smooth path between  $|\text{GS}_{f,X}\rangle$  and  $|\text{VBS}_{f,X'}\rangle$  can always be explicitly constructed by smoothly deforming every CLS in  $X$  to one single site while preserving the  $\text{SO}(3)$  or  $\text{SO}(3) \times \text{trn}$  symmetry, and thus the two states always represent the same phase protected by the symmetry. Let  $|\text{GS}_{2,\square}\rangle$  be the ground state of spin-2 bosons in the 2D Tasaki lattice, for the above reason,  $|\text{GS}_{2,\square}\rangle$  and  $|\text{VBS}_{2,\square}\rangle$  are in the same SPT phase protected by  $\text{SO}(3) \times \text{trn}$ .

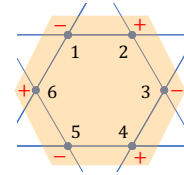


FIG. 7. A CLS in the kagome lattice. Sign of the amplitude alternates from site 1 to 6.

In terms of crystalline symmetries, however, situations can be different. For simplicity, we only consider point group symmetries in  $d = 2$  dimension in this article. Let  $G$  be a point group of a Hamiltonian with a unique ground state  $|\Psi\rangle$ . Let  $\hat{U}(q)$  be the symmetry operation (on the Hilbert space) corresponding to the group element  $q \in G$ . Subjected to  $q$ , the unique ground state transforms as,

$$|\Psi\rangle \rightarrow \hat{U}(q)|\Psi\rangle = e^{i\theta_q} |\Psi\rangle, \quad (35)$$

where the phase factors  $\{e^{i\theta_q}\}_{q \in G}$  form a 1D representation of  $G$ , and different 1D representations label different phases protected by the point group  $G$  [96]. When  $\{e^{i\theta_q}\}_{q \in G}$  is a trivial representation, that is,  $e^{i\theta_q} = 1$  for all  $q \in G$ ,  $|\Psi\rangle$  is in a trivial phase. On the other hand,  $|\Psi\rangle$  is in an SPT phase if  $\{e^{i\theta_q}\}_{q \in G}$  is a nontrivial representation. It is important to be aware that for

point group symmetries alone in  $d = 1, 2$  dimensions, the SPT/trivial classifications become meaningless when there are microscopic degrees of freedom lying precisely at symmetry centers. See Sec. IB of Ref. [97] or Appendix A of Ref. [70] for details. In other words, it is only legal to put the symmetry centers in vacuum.

In the graph representation of VBS states, we can assign an arbitrary direction to each singlet bond, because a singlet state is antisymmetric. Reversing the direction of a singlet bond is equivalent to adding a minus sign, see Fig. 8(a). Let us consider the point group  $D_2$  as a simple example. Elements in  $D_2$  are generated by two perpendicular mirror planes  $\sigma_1$  and  $\sigma_2$ , as shown in Fig. 8(b)-(c). Consider the states  $|\text{VBS}_{2,\square}\rangle$  and  $|\text{VBS}_{3,\Delta}\rangle$  in the thermodynamic limit.  $|\text{VBS}_{2,\square}\rangle$  is  $D_2$ -symmetric around the center of a plaquette, the center of a bond, or a site, while  $|\text{VBS}_{3,\Delta}\rangle$  is  $D_2$ -symmetric around the center of a bond or a site. As emphasized before, to classify their phases, it is illegal to put the symmetry center on a site. For  $|\text{VBS}_{2,\square}\rangle$  with a plaquette-centered  $D_2$  symmetry, there are even number [98] of singlet bonds being reversed by a mirror reflection [see Fig. 8(b)], thus  $\hat{U}(q)|\text{VBS}_{2,\square}\rangle = |\text{VBS}_{2,\square}\rangle$ ,  $\forall q \in D_2$ . However, for a bond-centered  $D_2$  symmetry, with respect to the mirror plane perpendicular to the central bond, there are odd number of singlet bonds being reversed, which results in a nontrivial representation of  $D_2$ . We see that in this example, the phase depends on the position of the symmetry center [99]. For some reason that will be clear later, we only consider the plaquette-centered symmetry for  $|\text{VBS}_{2,\square}\rangle$  in the remnant of this article. For  $|\text{VBS}_{3,\Delta}\rangle$ , the bond-centered symmetry is the only legal choice. As shown in Fig. 8(c), the mirror reflection  $\sigma_2$  reverses odd number of bonds, we thus have  $\hat{U}(\sigma_2)|\text{VBS}_{3,\Delta}\rangle = -|\text{VBS}_{3,\Delta}\rangle$ . As listed in Fig. 8(d),  $|\text{VBS}_{2,\square}\rangle$  results in a trivial representation of plaquette-centered  $D_2$  and is therefore in a trivial phase, while  $|\text{VBS}_{3,\Delta}\rangle$  is in an SPT phase protected by  $D_2$ . Note that from the above discussion, one might naively think that one single mirror plane alone (point group  $D_1$ ) is sufficient to distinguish the SPT from the trivial phase, which is indeed true in  $d = 1, 3$  dimensions [5, 70]. However, in  $d = 2$ ,  $D_1$  symmetry can only give a trivial phase, see Ref. [97].

In general, the smooth path (between  $|\text{GS}_{f,X}\rangle$  and  $|\text{VBS}_{f,X'}\rangle$ ) mentioned before may or may not break crystalline symmetries. For example, by smoothly deforming every CLS into the single site at its center,  $|\text{GS}_{2,\mathbb{D}}\rangle$  reduces to  $|\text{VBS}_{2,\square}\rangle$  while preserving the plaquette-centered  $D_2$  symmetry, see Fig. 6(a). (Though  $|\text{GS}_{2,\mathbb{D}}\rangle$  also has site-centered  $D_2$  symmetry, such symmetry does not give a phase classification.) For  $|\text{GS}_{3,\star}\rangle$ , however, the smooth path described by Eq. (34) breaks the  $D_2$  symmetry. In general, when we are not able to find a path that is both crystalline-symmetry-preserving and smooth, such path either is too complicated to be explicitly found or simply does not exist. Nevertheless, it is always possible to investigate the crystalline-symmetry-protected phase of  $|\text{GS}_{f,X}\rangle$  case-by-case. We again use

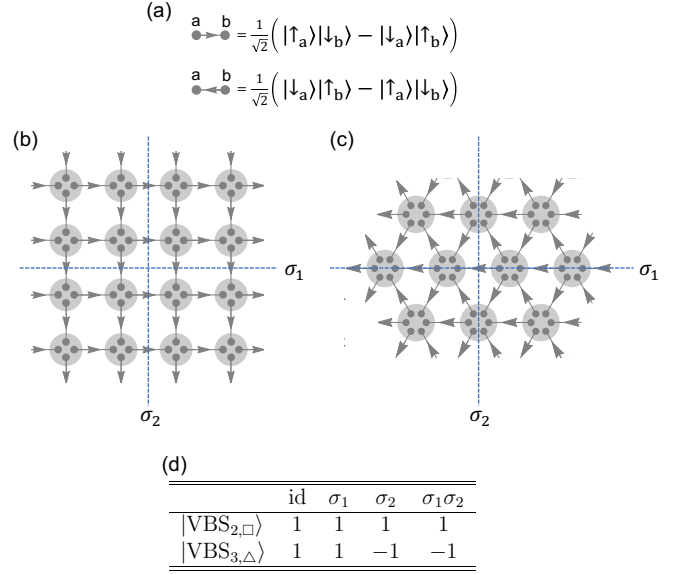


FIG. 8. (a) A direction can be assigned to each singlet bond. Two opposite directions differ by a minus sign. (b)  $|\text{VBS}_{2,\square}\rangle$  is invariant under reflections about mirror planes  $\sigma_1$  and  $\sigma_2$ . We assume the symmetry center lies in a plaquette. (c)  $|\text{VBS}_{3,\Delta}\rangle$  is invariant under reflections about mirror planes  $\sigma_1$  and  $\sigma_2$ . (d)  $|\text{VBS}_{2,\square}\rangle$  results in a trivial representation of  $D_2 = \{\text{id}, \sigma_1, \sigma_2, \sigma_1\sigma_2\}$  (plaquette-centered), while  $|\text{VBS}_{3,\Delta}\rangle$  results in a nontrivial representation of  $D_2$  (bond-centered).

$|\text{GS}_{3,\star}\rangle$  as an example. As shown in Fig. 9(a), we put the symmetry center at the geometric center of a hexagonal plaquette. A CLS in the kagome lattice can actually be regarded as a 0-dimensional SPT phase protected by  $D_2$ , because, for example, according to Eq. (32) and Fig. 7,  $\hat{U}(\sigma_2)\hat{B}_{1,\alpha}^{3,\star}\hat{U}(\sigma_2) = -\hat{B}_{1,\alpha}^{3,\star}$ . The many-body ground state  $|\text{GS}_{3,\star}\rangle$  is a fully packing of CLSs with entangled spins. The spin configurations of  $|\text{GS}_{3,\star}\rangle$ , which is inherited from  $|\text{VBS}_{3,\Delta}\rangle$ , transforms trivially, as shown in Fig. 9(b)-(c). (Note that Fig. 9(b) does not imply that  $|\text{VBS}_{3,\Delta}\rangle$  is in a trivial phase protected by  $D_2$ , as the symmetry is site-centered.) Nevertheless,  $|\text{GS}_{3,\star}\rangle$  yields a nontrivial representation of  $D_2$  thanks to how CLSs transform. We thus see that  $|\text{GS}_{3,\star}\rangle$  is in an SPT phase protected by  $D_2$ ; the SPT phase is purely a result of charge fluctuations at zero temperature, as the spin degrees of freedom contribute trivially. Similarly, with the symmetry center in Fig. 9(a), one can also show that  $|\text{GS}_{3,\star}\rangle$  represents an SPT phase protected by point group  $D_6$ , while  $D_6$  is not a proper symmetry for the phase of  $|\text{VBS}_{3,\Delta}\rangle$ , since the VBS state is  $D_6$  invariant only about a site. Once again, the SPT phase of  $|\text{GS}_{3,\star}\rangle$  protected by  $D_6$  originates from the charge fluctuations of each CLS.

Table III and IV summarize the results in this section. For a specific symmetry, to identify the phase of  $|\text{GS}_{f,X}\rangle$ , we first try to find a both symmetry-preserving and smooth path that connects  $|\text{GS}_{f,X}\rangle$  to  $|\text{VBS}_{f,X'}\rangle$ ,

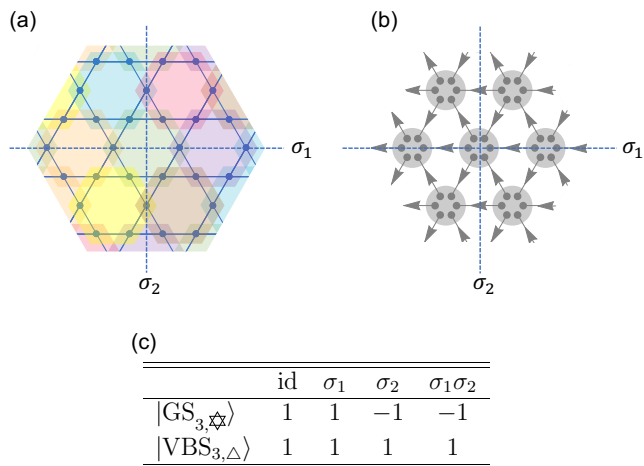


FIG. 9. (a) A FPS on the kagome lattice. ( $|\text{GS}_{3,\star}\rangle$  is  $D_2$  symmetric, and it is a superposition of FPSs with different spin configurations.) We require that the symmetry center of  $D_2$  lies at the geometric center of a hexagon. (b) For  $|\text{VBS}_{3,\Delta}\rangle$ , the symmetry center should lie at a site (spin) in order to be compatible with (a). (c) 1D representations of  $D_2$  associated with  $|\text{GS}_{3,\star}\rangle$  and  $|\text{VBS}_{3,\Delta}\rangle$ . Note that the latter state transforms trivially, but this does not mean that it is in a trivial phase.

provided that the phase of  $|\text{VBS}_{f,X'}\rangle$  is already known. (For point group symmetries, we require that there are no microscopic degrees of freedom lying at the symmetry center anywhere along the path [100].) When such a path cannot be explicitly found, it is either too complicated to be found or simply absent. Nevertheless, for point group symmetries, based on Eq. (35) we can always classify the phase of  $|\text{GS}_{f,X}\rangle$  without the help of the smooth path argument. Note that for two reasons, the classifications presented in Table III and IV should not be considered as complete results. First, we have seen that the phase of  $|\text{GS}_{f,X}\rangle$  is highly related to  $|\text{VBS}_{f,X'}\rangle$ . However, in  $d > 1$  dimensions, a systematic classification of  $|\text{VBS}_{f,X'}\rangle$  with respect to all of its symmetry groups is absent [101]. Second, the present classification theories of SPT phases in  $d > 1$  are incomplete. In other words, there might be unknown symmetries that give rise to SPT/trivial classifications.

	SO(3)	SO(3) $\times$ trn	$D_2$
$ \text{VBS}_{2,\square}\rangle$	trivial	<b>SPT</b>	trivial
$ \text{GS}_{2,\mathbb{D}}\rangle$	trivial	<b>SPT</b>	trivial

TABLE III. Classifying the symmetry-protected phases of  $|\text{VBS}_{2,\square}\rangle$  and  $|\text{GS}_{2,\mathbb{D}}\rangle$  in terms of different symmetries. Here  $D_2$  is assumed to be a plaquette-centered symmetry.

	SO(3)	SO(3) $\times$ trn	$D_2$	$D_6$
$ \text{VBS}_{3,\Delta}\rangle$	trivial	trivial	<b>SPT</b>	N/A
$ \text{GS}_{3,\star}\rangle$	trivial	trivial	<b>SPT</b>	<b>SPT</b>

TABLE IV. Classifying the symmetry-protected phases of  $|\text{VBS}_{3,\Delta}\rangle$  and  $|\text{GS}_{3,\star}\rangle$  in terms of different symmetries.

#### IV. SUMMARY

We show that the SPT phases can be realized with short-range interacting spinful bosons that are loaded on lattices with a bottom flat band. Such systems are described by the spinful Bose-Hubbard models. The ground states of such systems have both spin and charge fluctuations. The single-body eigenstates of a flat band can usually be chosen to be strictly localized on finite sites, known as compact localized states (CLSs). When  $N$  spin- $f$  bosons are loaded on a bottom-flat-band lattice  $X$  with  $N$  unit cells, at low temperatures, the particles' wave functions tend to avoid overlapping each other in order to minimize the system's energy. Especially, when the interaction strength between spin- $f$  bosons is fine-tuned, in the ground state  $|\text{GS}_{f,X}\rangle$ ,  $N$  bosons exactly occupy  $N$  CLSs on different patches. This enables us to exactly map  $|\text{GS}_{f,X}\rangle$  onto  $|\text{VBS}_{f,X'}\rangle$ , where the latter state is the spin- $f$  VBS state on the lattice  $X'$ . This implies that  $|\text{GS}_{f,X}\rangle$  is the exact and unique many-body ground state. The choice of  $f$  and  $X'$  is determined by the geometry of  $X$ . For example, when  $X =$  sawtooth chain, one should take  $f = 1$  and  $X' =$  simple 1D chain, see Sec II. As another example, if  $X =$  kagome lattice, we should choose  $f = 3$  and  $X' =$  triangular lattice, see Sec. III B.

The spin fluctuations of  $|\text{GS}_{f,X}\rangle$  is inherited from  $|\text{VBS}_{f,X'}\rangle$ . Therefore, with respect to the spin rotation symmetry or the combination of spin rotation and translation symmetry, the symmetry-protected phase of  $|\text{GS}_{f,X}\rangle$  is identical to that of  $|\text{VBS}_{f,X'}\rangle$ . However, unlike  $|\text{VBS}_{f,X'}\rangle$ , the state  $|\text{GS}_{f,X}\rangle$  also possesses non-vanishing charge fluctuations, and in terms of crystalline symmetries, both spin and charge fluctuations in  $|\text{GS}_{f,X}\rangle$  together determine its symmetry-protected phase. Hence, one cannot simply conclude that the crystalline-symmetry-protected phase of  $|\text{GS}_{f,X}\rangle$  is also inherited from  $|\text{VBS}_{f,X'}\rangle$ , because charge fluctuations may play a nontrivial role in the former state, which is indeed the case for spin-3 bosons in the kagome lattice.

Although our analysis in  $d > 1$  dimensions is based on the exact ground states  $|\text{GS}_{f,X}\rangle$  (as a consequence of fine-tuned parameters), we expect that just like what has been shown in the spin-1 BHMSC, the symmetry-protected phase survives in rather wide parameter regions, and  $|\text{GS}_{f,X}\rangle$  serves as a representative state of the phase.

## ACKNOWLEDGMENTS

We acknowledge stimulating discussions with Hal Tasaki, Syngae Todo, and Lin-hao Li. H. Y. was supported by Grant-in-Aid for JSPS Research Fellowship for Young Scientists (DC1) No. 20J20715. H. N. was supported by the Advanced Leading Graduate Course for Photon Science (ALPS) at the University of Tokyo. H. K. was supported in part by JSPS Grant-in-Aid for Scientific Research on Innovative Areas No. JP20H04630, JSPS KAKENHI Grant No. JP18K03445, and the Inamori Foundation.

### Appendix A: The Haldane insulator phase

Spinless bosons in optical lattices with dipole-dipole interaction are described by the extended Bose-Hubbard model. The Haldane insulator phase in the 1D extended Bose-Hubbard model can be captured by the following state [13]:

$$|\Psi_{\text{HI}}\rangle = \prod_j (\hat{a}_j^\dagger + \hat{a}_{j+1}^\dagger) |\text{vac}\rangle, \quad (\text{A1})$$

where  $\hat{a}_j^\dagger$  creates a spinless boson at site  $j$ . See Fig. 10(a). The state  $|\Psi_{\text{HI}}\rangle$  represents a trivial phase in the sense of inversion symmetry, but it represents a Haldane phase protected by the combination of pseudo-spin rotation and the inversion symmetry, i.e., the group  $\{1, \hat{U}(n\mathcal{I})\}$  with  $\hat{U}(n\mathcal{I}) := \exp[-i\pi \sum_r (\hat{n}_r - 1)] \hat{U}(\mathcal{I})$ . This is the same for  $|\text{GS}_{\lambda=0}\rangle$ , see Table I. In addition, the Haldane phase of  $|\text{GS}_{\lambda=0}\rangle$  is protected by other symmetries related to the spin degree of freedom. In this sense, we can say the state  $|\text{GS}_{\lambda=0}\rangle$  represents a spinful Haldane insulator phase. Note that both  $|\Psi_{\text{HI}}\rangle$  and  $|\text{GS}_{\lambda=0}\rangle$  exhibit perfect hidden charge order, i.e., vacant sites and doubly occupied sites appear alternatively if we ignore all the singly occupied sites.

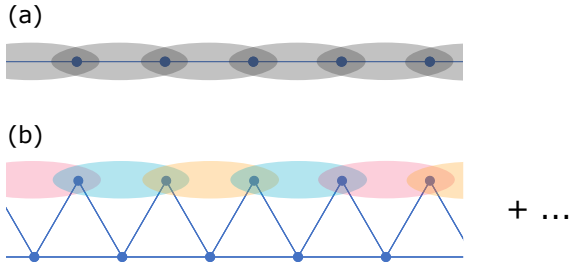


FIG. 10. (a) The Haldane insulator phase in the 1D system of spinless bosons. Every ellipse represents a single particle. (b) The state  $|\text{GS}\rangle$  at  $\lambda = 0$ . Three different colors denote three different spin states, and all allowed spin configurations are summed up (with coefficients).

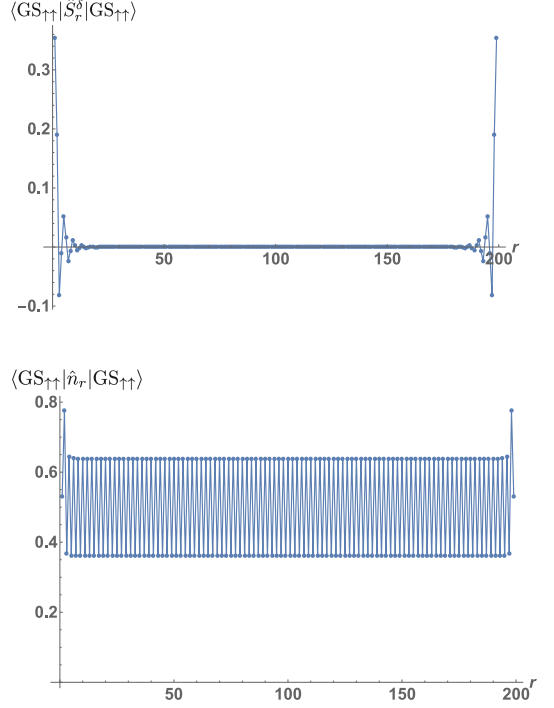


FIG. 11. Spin and charge edge states. We have assumed that the sawtooth chain ends with bottom sites at both ends and taken  $N = 100$  and  $\lambda = 1$ .

### Appendix B: Spin and charge edge states

For spin-1 BHMSC with OBC,  $g_0^t = 0$  and  $g_2^t > 0$ , there are four degenerate ground states  $|\text{GS}_{\uparrow\uparrow}\rangle$ ,  $|\text{GS}_{\uparrow\downarrow}\rangle$ ,  $|\text{GS}_{\downarrow\uparrow}\rangle$ , and  $|\text{GS}_{\downarrow\downarrow}\rangle$ , which correspond to four independent edge spin-1/2 states. The analytical forms of  $\langle \text{GS}_{\uparrow\uparrow} | \hat{S}_r^\delta | \text{GS}_{\uparrow\uparrow} \rangle$ ,  $\langle \text{GS}_{\uparrow\uparrow} | \hat{n}_r | \text{GS}_{\uparrow\uparrow} \rangle$ , etc. are rather complicated and will not be presented. Instead, their plots are shown in Fig. 11. The spin edge state decays more slowly than the charge one, because the spin correlation length is longer than the charge correlation length:

$$\xi_{\text{spin}} = \left( \ln \frac{3\lambda^2 + \sqrt{9\lambda^4 + 36\lambda^2 + 24} + 6}{\lambda^2 + \sqrt{\lambda^4 + 4\lambda^2 + 24} + 2} \right)^{-1}, \quad (\text{B1})$$

$$\xi_{\text{charge}} = \left( \ln \frac{3\lambda^2 + \sqrt{9\lambda^4 + 36\lambda^2 + 24} + 6}{3\lambda^2 - \sqrt{9\lambda^4 + 36\lambda^2 + 24} + 6} \right)^{-1}.$$

There is always a spin-1/2 localized at each edge. We define the reduced edge particle number as  $\bar{N}_{\text{edge}} := \sum_{r=1}^{\infty} (\lim_{N \rightarrow \infty} \langle \text{GS}_{\uparrow\uparrow} | \hat{n}_r | \text{GS}_{\uparrow\uparrow} \rangle - 1/2)$ .  $\bar{N}_{\text{edge}}$  is a function of  $\lambda$ , and  $\bar{N}_{\text{edge}} = 1/2$  at  $\lambda = 0$ . See Fig. 12. Note that  $\bar{N}_{\text{edge}}$  is independent of the four degenerate ground states.

Let us note that for crystalline-symmetry-protected topological phases in  $d = 1, 2$  dimensions, there are no anomalous edge states [97]. For example, both  $|\text{GS}_{3, \star}\rangle$  and  $|\text{VBS}_{3, \Delta}\rangle$  are protected by  $D_2$  symmetry (see Sec. III), and they do not have anomalous edge states.

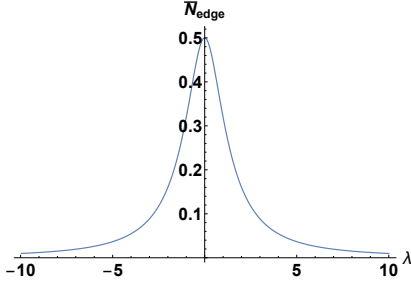


FIG. 12. The reduced edge particle number  $\bar{N}_{\text{edge}}$  as a function of  $\lambda$ .

### Appendix C: Kennedy-Tasaki transformation for integer-spin itinerant systems

Kennedy-Tasaki transformation is a nonlocal unitary transformation defined on an open chain of length  $L$  as [5, 7–9]

$$\hat{U}_{\text{KT}} := \prod_{j=1}^L \exp \left[ i\pi \left( \sum_{i=1}^{j-1} \hat{S}_i^z \right) \hat{S}_j^x \right], \quad (\text{C1})$$

and it is hermitian:  $\hat{U}_{\text{KT}}^\dagger = \hat{U}_{\text{KT}}$ .  $\hat{U}_{\text{KT}}$  is also invariant under  $\mathbb{Z}_2 \times \mathbb{Z}_2$  spin rotation. For an arbitrary integer-spin chain, let  $\hat{h}_j$  be a local Hamiltonian, the sufficient and necessary condition for  $\hat{U}_{\text{KT}} \hat{h}_j \hat{U}_{\text{KT}}$  to be also local is that  $\hat{h}_j$  is  $\mathbb{Z}_2 \times \mathbb{Z}_2$  invariant [4, 9]. This statement can be extended to integer-spin itinerant systems. For example, the spin-1 Bose-Hubbard model has  $\text{SO}(3)$  spin rotation symmetry, and the on-site interaction  $\hat{P}_r^{(S)}$  is invariant under  $\hat{U}_{\text{KT}}$ , while the  $\text{SO}(3)$ -invariant hopping transforms as

$$\begin{aligned} & \hat{U}_{\text{KT}} \left( \sum_{\alpha=0,\pm 1} \hat{a}_{i,\alpha}^\dagger \hat{a}_{j,\alpha} + \text{h.c.} \right) \hat{U}_{\text{KT}} \\ &= e^{i\pi \sum_{v=i}^{j-1} \hat{S}_v^z} a_{i,0}^\dagger \hat{a}_{j,0} + \text{h.c.} \\ &+ \frac{1}{2} e^{i\pi \sum_{v=i+1}^j \hat{S}_v^z} \left[ \left( e^{i\pi \sum_{u=i}^{j-1} \hat{S}_u^z} + 1 \right) \left( a_{i,+}^\dagger \hat{a}_{j,+} + a_{i,-}^\dagger \hat{a}_{j,-} \right) \right. \\ &+ \left. \left( e^{i\pi \sum_{u=i}^{j-1} \hat{S}_u^z} - 1 \right) \left( \hat{a}_{i,+}^\dagger a_{j,-} + \hat{a}_{i,-}^\dagger \hat{a}_{j,+} \right) \right] + \text{h.c.} \end{aligned} \quad (\text{C2})$$

We can see that the transformed hopping has  $\mathbb{Z}_2 \times \mathbb{Z}_2$  symmetry and is still local if the original hopping is local.

### Appendix D: Translation symmetry and the Haldane phases

In the presence of both translation symmetry and  $\mathbb{Z}_2 \times \mathbb{Z}_2$  symmetry,  $\{\phi_q\}_{q \in \mathbb{Z}_2 \times \mathbb{Z}_2}$  in Eq. (22) forms a 1D representation of the group  $\mathbb{Z}_2 \times \mathbb{Z}_2$ . In this case, all the

phases of gapped states that do not break the two symmetries are classified by a pair of indices  $(\omega, \gamma)$  where  $\omega \in \mathcal{Q}_{\mathbb{Z}_2 \times \mathbb{Z}_2}$  and  $\gamma$  labels different 1D representations of  $\mathbb{Z}_2 \times \mathbb{Z}_2$  [72]; see Table V. Let us again use the sawtooth chain as an example. It is easy to see that the state  $|\text{GS}\rangle$  in Eq. (19) corresponds to the row  $\gamma = 1$  in Table V. We now show that other three SPT phases labeled by  $(\omega = -1, \gamma = x, y, z)$  can be obtained by slightly modifying  $\hat{H}_{\text{hop}}$ . Define

$$\hat{W}^\gamma := \prod_{k=1}^{N/4} e^{-i\pi(\hat{S}_{4k-1}^\gamma + \hat{S}_{4k}^\gamma)}, \quad \gamma = x, y, z. \quad (\text{D1})$$

The operator  $\hat{W}^\gamma$  acts on the red sites pictured in Fig. 13. Interaction  $\hat{H}_{\text{int}}$  is invariant under  $\hat{W}^\gamma$ , thus  $\hat{H}^\gamma := \hat{W}^\gamma \hat{H} \hat{W}^\gamma = \hat{W}^\gamma \hat{H}_{\text{hop}} \hat{W}^\gamma + \hat{H}_{\text{int}}$ . The transformation does not break the translation symmetry. The unique ground state of  $\hat{H}^\gamma$  is given by

$$\begin{aligned} |\text{GS}^\gamma\rangle &= \hat{W}^\gamma |\text{GS}\rangle \\ &= \sum_{\tau_1, \dots, \tau_{2N} = -1}^3 \text{Tr}(F^{\tau_1} E^{\tau_2} \Sigma^\gamma F^{\tau_3} E^{\tau_4} \Sigma^\gamma \dots) \times \\ &\quad \left( \prod_{r=1}^{2N} \hat{d}_{r,\tau_r}^\dagger \right) |\text{vac}\rangle, \end{aligned} \quad (\text{D2})$$

where  $\Sigma^\gamma := \text{diag}(\sigma^\gamma, \sigma^\gamma)$ . Under the  $\mathbb{Z}_2 \times \mathbb{Z}_2$  spin rotation, matrices in  $|\text{GS}^\gamma\rangle$  transforms as

$$F^{\tau_{2j-1}} E^{\tau_{2j}} \Sigma^\gamma \rightarrow e^{i\phi_q} u_q^\dagger F^{\tau_{2j-1}} E^{\tau_{2j}} \Sigma^\gamma u_q. \quad (\text{D3})$$

Unitary matrices  $\{u_q\}$  above are also given in Table I. Explicit calculation yields the other three different 1D representations of  $\mathbb{Z}_2 \times \mathbb{Z}_2$  in Table V. We thus have the desired SPT phases.

TABLE V. Four different 1D representations of  $\mathbb{Z}_2 \times \mathbb{Z}_2$ .

	$\phi_1$	$\phi_x$	$\phi_y$	$\phi_z$
$\gamma = 1$	+1	+1	+1	+1
$\gamma = x$	+1	+1	-1	-1
$\gamma = y$	+1	-1	+1	-1
$\gamma = z$	+1	-1	-1	+1

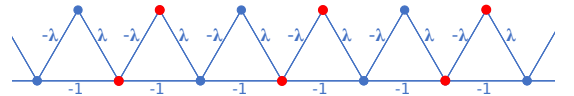


FIG. 13. Hopping constant  $t_{r,r'}$  for magnetic sublevel  $\pm 1$  in  $\hat{W}^\gamma \hat{H}_{\text{hop}} \hat{W}^\gamma$  when  $\gamma = z$ . Operator  $\hat{W}^\gamma$  acts on the red sites. One can see that the transformation  $\hat{W}^\gamma$  preserves the translation symmetry.

### Appendix E: MPS ansatz for numerical calculations

The MPS ansatz used in our numerical calculation can be regarded as a generalization of Eq. (19). For the matrices in Eq. (19), we can assign a pair of quantum numbers to each block as

$$\mathcal{F} := \sqrt{\lambda^2 + 2} \sum_{\tau=-1}^3 F^\tau \hat{a}_{r,\tau}^\dagger = \frac{1}{2} \begin{pmatrix} 0 & 1 \\ I_2 & -\lambda \sum_{\alpha} M^\alpha \hat{a}_{r,\alpha}^\dagger \\ 0 & I_2 \end{pmatrix},$$

$$\mathcal{E} := \sum_{\tau=-1}^3 E^\tau \hat{a}_{r,\tau}^\dagger = \frac{1}{2} \begin{pmatrix} 1/2 & 3/2 \\ \sum_{\alpha} M^\alpha \hat{a}_{r,\alpha}^\dagger & \sqrt{6} \hat{b}_r^\dagger I_2 \\ I_2 & \sum_{\alpha} M^\alpha \hat{a}_{r,\alpha}^\dagger \end{pmatrix}. \quad (\text{E1})$$

The quantum numbers are assigned by the following rule:

$$\begin{array}{c} n + m - 1/2 \\ \uparrow \\ n \rightarrow \text{a nonzero block that creates } m \text{ particles} \end{array} \quad (\text{E2})$$

---

$$\tilde{\mathcal{F}} = \begin{matrix} & 0 & \cdots & m & m+1 & \cdots & n-1 \\ 1/2 & \mathcal{X}_{[0]}^{(1)} & \cdots & \mathcal{X}_{[m]}^{(1)} & 0 & \cdots & 0 \\ 3/2 & 0 & \ddots & \ddots & \ddots & \ddots & \vdots \\ \vdots & \vdots & \ddots & \ddots & \ddots & \ddots & 0 \\ \vdots & \vdots & \ddots & \ddots & \ddots & \mathcal{X}_{[m]}^{(n-m)} & \\ \vdots & \vdots & \ddots & \ddots & \ddots & \vdots & \\ n - \frac{1}{2} & 0 & \cdots & \cdots & \cdots & 0 & \mathcal{X}_{[0]}^{(n)} \end{matrix}, \quad \tilde{\mathcal{E}} = \begin{matrix} & 1/2 & \cdots & m - \frac{1}{2} & m + \frac{1}{2} & \cdots & n - \frac{1}{2} \\ 0 & \mathcal{Y}_{[1]}^{(1)} & \cdots & \mathcal{Y}_{[m]}^{(1)} & 0 & \cdots & 0 \\ 1 & \mathcal{Y}_{[0]}^{(1)} & \ddots & \ddots & \ddots & \ddots & \vdots \\ 2 & 0 & \ddots & \ddots & \ddots & \ddots & 0 \\ \vdots & \vdots & \ddots & \ddots & \ddots & \mathcal{Y}_{[m]}^{(n-m+1)} & \\ \vdots & \vdots & \ddots & \ddots & \ddots & \vdots & \\ n-1 & 0 & \cdots & \cdots & 0 & \mathcal{Y}_{[0]}^{(n-1)} & \mathcal{Y}_{[1]}^{(n)} \end{matrix}, \quad (\text{E4})$$

where  $\mathcal{X}_{[k]}$  and  $\mathcal{Y}_{[k]}$  denote  $d \times d$  blocks that create  $k$  particles, and the maximum particle number on each site is truncated to  $m$ . The bond dimension is  $\chi = dn$ . The MPS  $|\Psi(\tilde{\mathcal{E}}, \tilde{\mathcal{F}})\rangle := \text{Tr}(\dots \tilde{\mathcal{E}} \tilde{\mathcal{F}} \tilde{\mathcal{E}} \tilde{\mathcal{F}} \dots) |\text{vac}\rangle$  is called a symmetric uniform MPS (suMPS) [73]. In our numerical calculations, we fix  $m = 3$ ,  $n = 4$  and vary  $d$ . We optimize the suMPS by minimizing its energy expectation value, and the optimization is done by the VUMPS algorithm.

Now we justify the particle number truncation  $m = 3$ . The energy variance of the MPS  $|\Psi(\tilde{\mathcal{E}}, \tilde{\mathcal{F}})\rangle$  is measured by

$$\begin{aligned} \sigma^2 &:= \frac{1}{N} \left( \langle \Psi(\tilde{\mathcal{E}}, \tilde{\mathcal{F}}) | \hat{H}^2 | \Psi(\tilde{\mathcal{E}}, \tilde{\mathcal{F}}) \rangle - \langle \Psi(\tilde{\mathcal{E}}, \tilde{\mathcal{F}}) | \hat{H} | \Psi(\tilde{\mathcal{E}}, \tilde{\mathcal{F}}) \rangle^2 \right) \\ &= \frac{1}{N} \langle \Psi(\tilde{\mathcal{E}}, \tilde{\mathcal{F}}) | \hat{H} \left( 1 - \hat{P}_{\tilde{\mathcal{E}}, \tilde{\mathcal{F}}} \right) \hat{H} | \Psi(\tilde{\mathcal{E}}, \tilde{\mathcal{F}}) \rangle, \end{aligned} \quad (\text{E5})$$

For example, the upper right block of  $\mathcal{E}$  creates two particles, thus the block is labeled by  $(0, 3/2)$ . For the product of  $2N$  matrices, we replace  $1/2$  in the above rule with  $2N/2 = N$ , such that

$$\underbrace{\mathcal{E} \mathcal{F} \mathcal{E} \mathcal{F} \dots \mathcal{E} \mathcal{F}}_{2N} = \frac{1}{1} \begin{pmatrix} 0 & 1 \\ \mathcal{X}_{11} & \mathcal{X}_{12} \\ \mathcal{X}_{21} & \mathcal{X}_{22} \end{pmatrix}, \quad (\text{E3})$$

where  $\mathcal{X}_{11}$  and  $\mathcal{X}_{22}$  are  $2 \times 2$  blocks which create  $N$  particles, while  $\mathcal{X}_{12}$  and  $\mathcal{X}_{21}$  create  $N + 1$  and  $N - 1$  particles, respectively. In the thermodynamic limit  $N \rightarrow \infty$ , Eq. (E3) gives an MPS where the particle number equals the number of unit cells.

The exact ground state given by Eq. (E3) has bond dimension  $\chi = 4$ . In general, however, we need to use an MPS with larger bond dimension to better approximate the true ground state. We can thus generalize Eq. (E1) to a block-banded form:

where  $\hat{P}_{\tilde{\mathcal{E}}, \tilde{\mathcal{F}}} := |\Psi(\tilde{\mathcal{E}}, \tilde{\mathcal{F}})\rangle \langle \Psi(\tilde{\mathcal{E}}, \tilde{\mathcal{F}})|$ . Let

$$\mathbb{H}_r^{\leq m} = \text{span} \left( \left\{ \prod_{\alpha=-1}^1 (\hat{a}_{r,\alpha}^\dagger)^{n_\alpha} |\text{vac}\rangle_r \mid \sum_{\alpha} n_\alpha \leq m \right\} \right) \quad (\text{E6})$$

be the local truncated Hilbert space and  $\hat{P}_{V \leq m}$  be the projection operator onto the total truncated Hilbert space  $\mathbb{H}^{V \leq m} := \bigotimes_{i=r}^{2N} \mathbb{H}_i^{\leq m}$ . The Hamiltonian in  $\mathbb{H}^{V \leq m}$  reads  $\hat{H}_{V \leq m} := \hat{P}_{V \leq m} \hat{H} \hat{P}_{V \leq m}$ . Equation (E5) can thus be rewritten as

$$\begin{aligned} \sigma^2 &= \frac{1}{N} \langle \Psi(\tilde{\mathcal{E}}, \tilde{\mathcal{F}}) | \hat{H}_{V \leq m} \left( 1 - \hat{P}_{\tilde{\mathcal{E}}, \tilde{\mathcal{F}}} \right) \hat{H}_{V \leq m} | \Psi(\tilde{\mathcal{E}}, \tilde{\mathcal{F}}) \rangle \\ &\quad + \frac{1}{N} \langle \Psi(\tilde{\mathcal{E}}, \tilde{\mathcal{F}}) | \hat{H} \left( 1 - \hat{P}_{V \leq m} \right) \hat{H} | \Psi(\tilde{\mathcal{E}}, \tilde{\mathcal{F}}) \rangle. \end{aligned} \quad (\text{E7})$$

The first term above can be viewed as the variance in

$\mathbb{H}^{\vee \leq m}$ , and it quantifies the effect of finite bond dimension. Similar to spin or fermion systems, the first term can be calculated efficiently [51, 102]. On the other hand, the second term quantifies the effect of truncation. Note that although  $\hat{H}(1 - \hat{P}_{\vee \leq m})\hat{H}$  contains  $\mathcal{O}(N^2)$  non-local terms, only  $\mathcal{O}(N)$  local terms return nonzero values when sandwiched by  $|\Psi(\tilde{\mathcal{E}}, \tilde{\mathcal{F}})\rangle$ . Table VI shows that for  $m = 3$ , at least near the Haldane-critical phase transition point, the effect of particle number truncation is about 100 times smaller than the effect of finite bond dimension.

TABLE VI. Some examples of the actual values of the first and second terms in Eq. (E7) with  $m = 3$ ,  $d = 100$ ,  $\lambda = 1$ , and  $R = 1$ . The Haldane-critical phase transition happens between  $\varphi = 6/36$  and  $7/36$ , see Fig. 2(b).

$\varphi/\pi$	first	second
1/36	1.144e-04	8.082e-05
2/36	3.463e-04	1.190e-04
3/36	9.122e-04	1.267e-04
4/36	1.957e-03	1.142e-04
5/36	3.543e-03	9.620e-05
6/36	5.702e-03	7.819e-05
7/36	7.348e-03	6.284e-05
8/36	8.614e-03	5.209e-05
9/36	8.956e-03	4.874e-05

Finally, we provide further numerical evidence that determines the shape of the phase boundary in the  $\lambda = 1$  plane in Fig. 2(a). The transfer matrix is defined as the sum of Kronecker products  $\sum_{\tau, \tau'} \tilde{E}^\tau \tilde{F}^{\tau'} \otimes \tilde{E}^\tau \tilde{F}^{\tau'}$ , where  $\tilde{E}^\tau := \langle \tau | \tilde{\mathcal{E}} | \text{vac} \rangle$  and  $\tilde{F}^{\tau'} := \langle \tau' | \tilde{\mathcal{F}} | \text{vac} \rangle$  with  $\{|\tau\rangle\}$  being a basis in the Fock space. Let  $\epsilon_i = -\ln |\lambda_i|$ , where  $\lambda_i$  is the  $i$ th largest absolute eigenvalue of the transfer matrix, and  $|\lambda_1|$  is normalized to 1. As we change the bond dimension  $\chi$ , we calculate the scaling of the inverse correlation length  $1/\xi := \epsilon_2$  with respect to  $\epsilon_3 - \epsilon_2$  along the path parameterized by  $(R \sin \varphi, R \cos \varphi, 1)$ , see Fig. 14. We find that, as  $R$  grows, the phase transition occurs at smaller  $\varphi$ , which indicates that the phase boundary is curved instead of straight.

### Appendix F: Uniqueness of the ground state of $\hat{H}^{f,X}$

Mathematically, the uniqueness of the exact ground state of  $\hat{H}^{f,X}$  can be proved with additional assumptions:  $\Lambda_X^{[1]} \neq \emptyset$  and  $g_{S,r} > 0$  for  $\forall S$  and  $\forall r \in \Lambda_X^{[1]}$ . With the ‘‘completeness relation’’  $\sum_S \hat{P}_r^{(S)} = \hat{n}_r(\hat{n}_r - 1)/2$  in mind and following the deduction in Eq. (10), one can show that the ground state can only be a linear combination of FPSs. The uniqueness of the ground state of  $\hat{H}^{f,X}$  then follows from the uniqueness of  $|\text{VBS}_{f,X'}\rangle$ . The assumption  $\Lambda_X^{[1]} \neq \emptyset$  is always satisfied in lattices generated by the cell construction, see, for example, Fig. 4(b) and Fig. 5(a). However, for the kagome lattice shown in

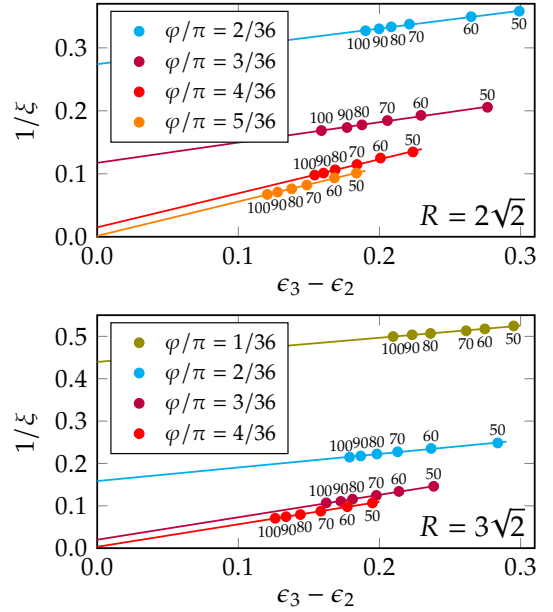


FIG. 14. Scaling of the inverse correlation length  $1/\xi := \epsilon_2$  with respect to  $\epsilon_3 - \epsilon_2$ . Numbers near the data points denote the corresponding bond dimensions  $d$  of each block. Along the path with  $R = 2\sqrt{2}$ , we see that a quantum phase transition occurs between  $\varphi = 4\pi/36$  and  $5\pi/36$ . On the other hand, along the path with  $R = 3\sqrt{2}$ , a phase transition occurs between  $\varphi = 3\pi/36$  and  $4\pi/36$ .

Fig. 5(b),  $\Lambda_X^{[1]} = \emptyset$ . Nevertheless, we propose the following conjecture: even in lattice  $X$  with  $\Lambda_X^{[1]} = \emptyset$ , the exact ground state of  $\hat{H}_X$  is unique when  $X'$  is not a bipartite lattice. For the kagome lattice,  $X'$  is a triangular lattice which is not bipartite. Note that if  $X'$  is bipartite and  $\Lambda_X^{[1]} = \emptyset$ , the ground state of  $\hat{H}^{f,X}$  will be degenerate. For example, for the Creutz ladder in Fig. 15(a), let  $(\hat{B}_{j,\beta_j}^{1,\boxtimes})^\dagger$  create a CLS of spin-1 boson, it is easy to see that the following two states both have zero energy:

$$\text{Tr} \prod_{j=1}^N \left[ \sum_{\beta_j} M^{\beta_j} \left( \hat{B}_{j,\beta_j}^{1,\boxtimes} \right)^\dagger \right] |\text{vac}\rangle, \quad (\text{F1a})$$

$$\prod_{\ell=1}^{N/2} \left[ \left( \hat{B}_{2\ell,0}^{1,\boxtimes} \right)^\dagger \left( \hat{B}_{2\ell,0}^{1,\boxtimes} \right)^\dagger - 2 \left( \hat{B}_{2\ell,1}^{1,\boxtimes} \right)^\dagger \left( \hat{B}_{2\ell,-1}^{1,\boxtimes} \right)^\dagger \right] |\text{vac}\rangle. \quad (\text{F1b})$$

These two states are depicted in Fig. 15(a). The first ‘‘nontrivial’’ state is a linear combination of FPSs, while the second state is a product state. Similar thing happens in spin-2 bosons loaded on the checkerboard lattice, see Fig. 15(b). In such cases, though the models  $\hat{H}^{f,X}$  do not exhibit any nontrivial phases due to the degeneracy, the ‘‘nontrivial’’ ground state (= the state which is a linear combination of FPSs) can always be regarded as the unique ground states of some other (usually more complicated) parent Hamiltonians [71], and hence the

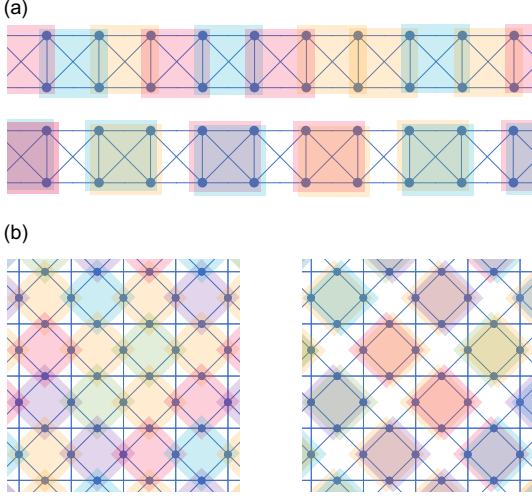


FIG. 15. A “nontrivial” ground state is degenerated with product states, if  $\Lambda_X^{[1]} = \emptyset$  and the corresponding quantum spin model lives on a bipartite lattice. (a) Spin-1 bosons on a Creutz ladder. Each colored square denotes a CLS with spin degree of freedom. Note that the ground states are superpositions of all allowed spin configurations. (b) Spin-2 bosons on a checkerboard lattice.  $X'$  in this case is a square lattice.

classification of such “nontrivial” states from the viewpoint of SPT phases still makes sense. For example, let  $|\text{GS}_{2,\square}\rangle$  be the “nontrivial” ground state of spin-2 bosons on the checkerboard lattice. Following the discussion in Sec. III C, by properly choosing the symmetry center and the mirror planes, one can show that  $|\text{GS}_{2,\square}\rangle$  is in an SPT phase protected by  $D_2$ . See Fig. 16.

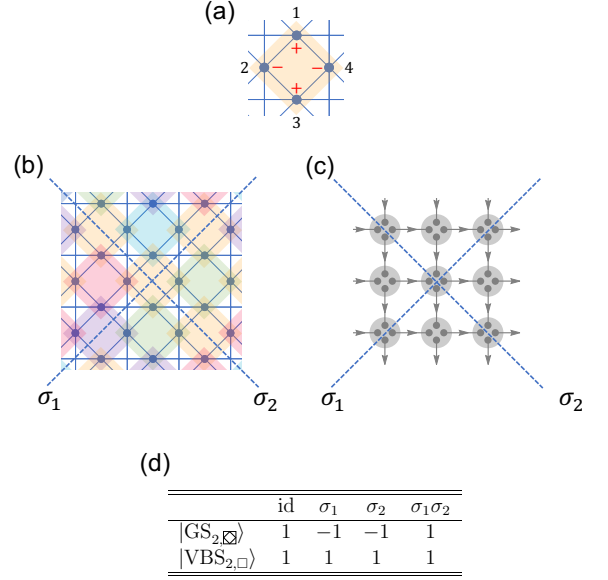
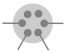


FIG. 16. (a) A CLS in the checkerboard lattice. Sign of the amplitude alternates from site 1 to 4. (b) A FPS on the checkerboard lattice. ( $|\text{GS}_{2,\square}\rangle$  is  $D_2$  symmetric, and it is a superposition of FPSs with different spin configurations.) We require that the symmetry center of  $D_2$  lies at the geometric center of a CLS and the two mirror planes are placed as in the figure. (c) For  $|\text{VBS}_{2,\square}\rangle$ , the symmetry center should lie at a site (spin) in order to be compatible with (b). (d) 1D representations of  $D_2$  associated with  $|\text{GS}_{2,\square}\rangle$  and  $|\text{VBS}_{2,\square}\rangle$ . The former state yields a nontrivial representation and is thus in an SPT phase.

- 
- [1] B. Zeng, X. Chen, D.-L. Zhou, and X.-G. Wen, *Quantum information meets quantum matter* (Springer, 2019).
  - [2] I. Affleck, T. Kennedy, E. H. Lieb, and H. Tasaki, *Phys. Rev. Lett.* **59**, 799 (1987).
  - [3] I. Affleck, T. Kennedy, E. H. Lieb, and H. Tasaki, *Commun. Math. Phys.* **115**, 477 (1988).
  - [4] F. Pollmann, A. M. Turner, E. Berg, and M. Oshikawa, *Phys. Rev. B* **81**, 064439 (2010).
  - [5] F. Pollmann, E. Berg, A. M. Turner, and M. Oshikawa, *Phys. Rev. B* **85**, 075125 (2012).
  - [6] Z.-C. Gu and X.-G. Wen, *Phys. Rev. B* **80**, 155131 (2009).
  - [7] H. Tasaki, *Physics and Mathematics of Quantum Many-Body Systems* (Springer, 2020).
  - [8] T. Kennedy and H. Tasaki, *Phys. Rev. B* **45**, 304 (1992).
  - [9] M. Oshikawa, *J. Phys. Condens. Matter* **4**, 7469 (1992).
  - [10] T. A. Hilker, G. Salomon, F. Grusdt, A. Omran, M. Boll, E. Demler, I. Bloch, and C. Gross, *Science* **357**, 484 (2017).
  - [11] S. de Léséleuc, V. Lienhard, P. Scholl, D. Barredo, S. Weber, N. Lang, H. P. Büchler, T. Lahaye, and A. Browaeys, *Science* **365**, 775 (2019).
  - [12] E. G. Dalla Torre, E. Berg, and E. Altman, *Phys. Rev. Lett.* **97**, 260401 (2006).
  - [13] E. Berg, E. G. Dalla Torre, T. Giamarchi, and E. Altman, *Phys. Rev. B* **77**, 245119 (2008).
  - [14] D. Rossini and R. Fazio, *New J. Phys.* **14**, 065012 (2012).
  - [15] J. Xu, Q. Gu, and E. J. Mueller, *Phys. Rev. Lett.* **120**, 085301 (2018).
  - [16] G. G. Batrouni, R. T. Scalettar, V. G. Rousseau, and B. Grémaud, *Phys. Rev. Lett.* **110**, 265303 (2013).
  - [17] S. Ejima, F. Lange, and H. Fehske, *Phys. Rev. Lett.* **113**, 020401 (2014).
  - [18] F. Lange, S. Ejima, and H. Fehske, *Phys. Rev. Lett.* **118**, 120401 (2017).
  - [19] M. Dalmonte, M. Di Dio, L. Barbiero, and F. Ortolani, *Phys. Rev. B* **83**, 155110 (2011).
  - [20] K. Sugimoto, S. Ejima, F. Lange, and H. Fehske, *Phys. Rev. A* **99**, 012122 (2019).
  - [21] J. Zhao, S. Hu, and P. Zhang, *Phys. Rev. Lett.* **115**, 195302 (2015).
  - [22] B. Grémaud and G. G. Batrouni, *Phys. Rev. B* **95**, 165131 (2017).

- [23] J. J. García-Ripoll, M. A. Martín-Delgado, and J. I. Cirac, *Phys. Rev. Lett.* **93**, 250405 (2004).
- [24] H. Nonne, P. Lecheminant, S. Capponi, G. Roux, and E. Boulat, *Phys. Rev. B* **81**, 020408 (2010).
- [25] V. Bois, S. Capponi, P. Lecheminant, M. Moliner, and K. Totsuka, *Phys. Rev. B* **91**, 075121 (2015).
- [26] S. Moudgalya and F. Pollmann, *Phys. Rev. B* **91**, 155128 (2015).
- [27] F. Lange, S. Ejima, and H. Fehske, *Phys. Rev. B* **92**, 041120 (2015).
- [28] M. Nakagawa and N. Kawakami, *Phys. Rev. B* **96**, 155133 (2017).
- [29] H. Ueda, T. Morimoto, and T. Momoi, *Phys. Rev. B* **98**, 045128 (2018).
- [30] P. Fromholz, S. Capponi, P. Lecheminant, D. J. Papoular, and K. Totsuka, *Phys. Rev. B* **99**, 054414 (2019).
- [31] S. Fazzini, L. Barbiero, and A. Montorsi, *Phys. Rev. Lett.* **122**, 106402 (2019).
- [32] A. Montorsi, S. Fazzini, and L. Barbiero, *Phys. Rev. A* **101**, 043618 (2020).
- [33] Y. Kawaguchi and M. Ueda, *Phys. Rep.* **520**, 253 (2012); D. M. Stamper-Kurn and M. Ueda, *Rev. Mod. Phys.* **85**, 1191 (2013).
- [34] H. Katsura and H. Tasaki, *Phys. Rev. Lett.* **110**, 130405 (2013).
- [35] H. Yang and H. Katsura, *Phys. Rev. Lett.* **122**, 053401 (2019).
- [36] A. Läuchli, G. Schmid, and S. Trebst, *Phys. Rev. B* **74**, 144426 (2006).
- [37] A. Browaeys, D. Barredo, and T. Lahaye, *J. Phys. B* **49**, 152001 (2016).
- [38] A. Eckardt, C. Weiss, and M. Holthaus, *Phys. Rev. Lett.* **95**, 260404 (2005).
- [39] A. Eckardt, P. Hauke, P. Soltan-Panahi, C. Becker, K. Sengstock, and M. Lewenstein, *Europhys. Lett.* **89**, 10010 (2010).
- [40] D. H. Dunlap and V. M. Kenkre, *Phys. Rev. B* **34**, 3625 (1986).
- [41] F. Grossmann, T. Dittrich, P. Jung, and P. Hänggi, *Phys. Rev. Lett.* **67**, 516 (1991).
- [42] F. Großmann and P. Hänggi, *Europhys. Lett.* **18**, 571 (1992).
- [43] K. Drese and M. Holthaus, *Phys. Rev. Lett.* **78**, 2932 (1997).
- [44] H. Lignier, C. Sias, D. Ciampini, Y. Singh, A. Zenesini, O. Morsch, and E. Arimondo, *Phys. Rev. Lett.* **99**, 220403 (2007).
- [45] A. Eckardt, M. Holthaus, H. Lignier, A. Zenesini, D. Ciampini, O. Morsch, and E. Arimondo, *Phys. Rev. A* **79**, 013611 (2009).
- [46] E. Kierig, U. Schnorrberger, A. Schietinger, J. Tomkovic, and M. K. Oberthaler, *Phys. Rev. Lett.* **100**, 190405 (2008).
- [47] A. Zenesini, H. Lignier, D. Ciampini, O. Morsch, and E. Arimondo, *Phys. Rev. Lett.* **102**, 100403 (2009).
- [48] J. Struck, C. Ölschläger, R. Le Targat, P. Soltan-Panahi, A. Eckardt, M. Lewenstein, P. Windpassinger, and K. Sengstock, *Science* **333**, 996 (2011).
- [49] J.-W. Rhim and B.-J. Yang, *Phys. Rev. B* **99**, 045107 (2019).
- [50] N. Read, *Phys. Rev. B* **95**, 115309 (2017).
- [51] V. Zauner-Stauber, L. Vanderstraeten, M. T. Fishman, F. Verstraete, and J. Haegeman, *Phys. Rev. B* **97**, 045145 (2018).
- [52] L. Vanderstraeten, J. Haegeman, and F. Verstraete, *SciPost Phys. Lect. Notes*, **7** (2019).
- [53] A. Imambekov, M. Lukin, and E. Demler, *Phys. Rev. A* **68**, 063602 (2003).
- [54] S. Tsuchiya, S. Kurihara, and T. Kimura, *Phys. Rev. A* **70**, 043628 (2004).
- [55] T.-L. Ho, *Phys. Rev. Lett.* **81**, 742 (1998); T. Ohmi and K. Machida, *J. Phys. Soc. Jpn.* **67**, 1822 (1998).
- [56] H. Tasaki, *Phys. Rev. Lett.* **69**, 1608 (1992).
- [57] H. Tasaki, *Prog. Theor. Phys.* **99**, 489 (1998).
- [58] K. Tamura and H. Katsura, *Phys. Rev. B* **100**, 214423 (2019).
- [59] T. Zhang and G.-B. Jo, *Sci. Rep.* **5**, 16044 (2015).
- [60] J. B. Parkinson, *J. Phys. C* **20**, L1029 (1987).
- [61] J. B. Parkinson, *J. Phys. C* **21**, 3793 (1988).
- [62] A. Mielke and H. Tasaki, *Comm. Math. Phys.* **158**, 341 (1993).
- [63] One can verify that the largest absolute eigenvalue of the transfer matrix  $\sum_{\tau, \tau'} F^\tau E^{\tau'} \otimes F^\tau E^{\tau'}$  is non-degenerate. This is equivalent to the statement that the MPS in Eq. (19) is injective.
- [64] Y.-T. Oh, H. Katsura, H.-Y. Lee, and J. H. Han, *Phys. Rev. B* **96**, 165126 (2017).
- [65] M. Andres, I. Schneider, and S. Eggert, *Phys. Rev. B* **77**, 014429 (2008).
- [66] Equation (22) is usually proved in the canonical form, see [103] or Theorem 7 in [104]. However, the equation holds regardless of the form of an injective MPS, see [7] or Section 7.3 in [105].
- [67] X. Chen, Z.-C. Gu, and X.-G. Wen, *Phys. Rev. B* **83**, 035107 (2011).
- [68] F. Pollmann and A. M. Turner, *Phys. Rev. B* **86**, 125441 (2012).
- [69] Y. Fuji, F. Pollmann, and M. Oshikawa, *Phys. Rev. Lett.* **114**, 177204 (2015).
- [70] H. Song, S.-J. Huang, L. Fu, and M. Hermele, *Phys. Rev. X* **7**, 011020 (2017).
- [71] D. Perez-Garcia, F. Verstraete, J. I. Cirac, and M. M. Wolf, arXiv preprint arXiv:0707.2260 (2007).
- [72] Z.-X. Liu, M. Liu, and X.-G. Wen, *Phys. Rev. B* **84**, 075135 (2011).
- [73] V. Zauner-Stauber, L. Vanderstraeten, J. Haegeman, I. P. McCulloch, and F. Verstraete, *Phys. Rev. B* **97**, 235155 (2018).
- [74] M. M. Rams, P. Czarnik, and L. Cincio, *Phys. Rev. X* **8**, 041033 (2018).
- [75] L. Tagliacozzo, T. R. de Oliveira, S. Iblisdir, and J. I. Latorre, *Phys. Rev. B* **78**, 024410 (2008).
- [76] S. R. Manmana, A. M. Läuchli, F. H. L. Essler, and F. Mila, *Phys. Rev. B* **83**, 184433 (2011).
- [77] A. N. Kirillov and V. E. Korepin, *Leningrad Math. J.* **1**, 343.
- [78] H. Katsura, N. Kawashima, A. N. Kirillov, V. E. Korepin, and S. Tanaka, *J. Phys. A* **43**, 255303 (2010).
- [79] T. Kennedy, E. H. Lieb, and H. Tasaki, *J. Stat. Phys.* **53**, 383 (1988).
- [80] A. Mielke, *Phys. Lett. A* **174**, 443 (1993).
- [81] A. Mielke, *J. Phys. A* **25**, 4335 (1992).
- [82] A. Mielke, *J. Phys. A* **24**, 3311 (1991).

- [83] L. Morales-Inostroza and R. A. Vicencio, *Phys. Rev. A* **94**, 043831 (2016).
- [84] W. Maimaiti, A. Andreanov, H. C. Park, O. Gendelman, and S. Flach, *Phys. Rev. B* **95**, 115135 (2017).
- [85] R. Dias and J. Gouveia, *Sci. Rep.* **5**, 16852 (2015).
- [86] A. Tanaka, *J. Stat. Phys.* (2020).
- [87] In fact, the sawtooth chain can be produced by either the cell construction or the line graph construction.
- [88] Z. Gulácsi, A. Kampf, and D. Vollhardt, *Phys. Rev. Lett.* **99**, 026404 (2007).
- [89] G.-B. Jo, J. Guzman, C. K. Thomas, P. Hosur, A. Vishwanath, and D. M. Stamper-Kurn, *Phys. Rev. Lett.* **108**, 045305 (2012).
- [90] Ignore spin for the moment, i.e., take  $f = 0$ . In  $d = 1$ ,  $N$  different CLSs can always be chosen to be linearly independent. However, in  $d > 1$  with PBC, these  $N$  CLSs can be linearly dependent in some cases, such as in kagome lattice [49]. Nevertheless, they can still be linearly independent in  $d > 1$  with OBC.
- [91] “On-site symmetry” is also called “internal symmetry”. It refers to a global symmetry that can be factorized site-by-site, and the symmetry operation on each site is an endomorphism of the on-site Hilbert space. The  $\mathbb{Z}_2 \times \mathbb{Z}_2$  spin rotation is an on-site symmetry because, for example,  $\hat{U}(z) = \prod_r \exp(-i\pi \hat{S}_r^z)$ , and  $\hat{S}_r^z$  acts only on the local Hilbert space.
- [92] See Refs. [1, 93, 94, 106, 107]. When the translation symmetry is indispensable to protect an SPT phase, such phase is often called a weak SPT phase.
- [93] X. Chen, Z.-X. Liu, and X.-G. Wen, *Phys. Rev. B* **84**, 235141 (2011).
- [94] S. Takayoshi, P. Pujol, and A. Tanaka, *Phys. Rev. B* **94**, 235159 (2016).
- [95] Consider  $|\text{VBS}_{3,\Delta}\rangle$  defined on a half-infinite plane. On its 1D boundary, every site hosts two “dangling” spin-1/2’s, as shown in the figure: . Since the six spin-1/2’s on the same site form a totally symmetric spin-3 degree of freedom, the two “dangling” spin-1/2’s have to form a symmetric spin-1 degree of freedom. One can add perturbations at the boundary that couple these spin-1’s through, for example, the translation invariant spin-1 AKLT Hamiltonian. This perturbation thus results in a gapped edge state without breaking the combination of SO(3) and translation symmetry, and hence the state  $|\text{VBS}_{3,\Delta}\rangle$  is in a trivial phase protected by such symmetry. A similar analysis for state  $|\text{VBS}_{2,\square}\rangle$  can be found in Refs. [1, 93, 94].
- [96] All 1D representations of  $G$  can form an Abelian group, which is the 1st cohomology group  $H^1[G, U(1)]$ . In  $d = 1, 2$  dimensions,  $H^1[G, U(1)]$  is believed to give a complete classification of phases protected by the point group  $G$ . In  $d = 3$  dimension, extra indices are needed for a complete classification. See Refs. [70, 97, 108] for general classification theories.
- [97] S.-J. Huang, H. Song, Y.-P. Huang, and M. Hermele, *Phys. Rev. B* **96**, 205106 (2017).
- [98] In the thermodynamic limit, it may be subtle to ask if the number is even or odd. Nevertheless, it is always possible to identify the phase of a finite-size system.
- The fact is that, the symmetry-protected phase of a finite-size system should be identical to that of an infinite system. The reason is as follows. All the symmetry-protected phases are about local properties of the system, since there is only short-range entanglement in the bulk [1]. In fact, according to Refs. [70, 97], the point-group-symmetry-protected phases of a 1D or 2D system are determined by the properties of a local region around the symmetry center, and the size of the local region roughly agrees with the correlation length. Local properties are obviously not affected by the those degrees of freedom that are infinitely far away.
- [99] How can the same point group in the same system results in two distinct phases by only shifting the symmetry center? The reason is that the plaquette-centered symmetry and the bond-centered symmetry are inequivalent in the sense that one symmetry alone does not imply the other. In the presence of translation symmetry, point groups centered in inequivalent positions are included in a larger space group (or wallpaper group). It is reasonable to say that the state  $|\text{VBS}_{2,\square}\rangle$  is in an SPT phase protected by the wallpaper group  $p4m$ , since bond-centered  $D_2$  is a subgroup of  $p4m$ . See Ref [97] for the theory of wallpaper-group-protected phases.
- [100] The state in Eq. (19) with  $0 < |\lambda| < \infty$  is inversion symmetric only about a site. In Table I, we can see that this path smoothly connects two different phases when the inversion symmetry is involved.
- [101] It is known that in  $d > 1$  dimensions, the combination of certain on-site and crystalline symmetries can also give rise to SPT/trivial classifications. So far most of our understandings of such combinations come from the Lieb-Schultz-Mattis (LSM) theorem and its generalizations, see Refs. [109–113] and the references therein. It is known that these LSM-type theorems are a special case of constraints at the boundary of SPT phases [107].
- [102] C. Hubig, J. Haegeman, and U. Schollwöck, *Phys. Rev. B* **97**, 045125 (2018).
- [103] D. Pérez-García, M. M. Wolf, M. Sanz, F. Verstraete, and J. I. Cirac, *Phys. Rev. Lett.* **100**, 167202 (2008).
- [104] D. Perez-Garcia, F. Verstraete, M. M. Wolf, and J. I. Cirac, *Quantum Info. Comput.* **7**, 401–430 (2007).
- [105] M. Fannes, B. Nachtergaele, and R. F. Werner, *Commun. Math. Phys.* **144**, 443 (1992).
- [106] X. Chen, Z.-C. Gu, Z.-X. Liu, and X.-G. Wen, *Phys. Rev. B* **87**, 155114 (2013).
- [107] M. Cheng, M. Zaletel, M. Barkeshli, A. Vishwanath, and P. Bonderson, *Phys. Rev. X* **6**, 041068 (2016).
- [108] R. Thorngren and D. V. Else, *Phys. Rev. X* **8**, 011040 (2018).
- [109] M. Oshikawa, *Phys. Rev. Lett.* **84**, 1535 (2000).
- [110] Y. Fuji, *Phys. Rev. B* **93**, 104425 (2016).
- [111] S. A. Parameswaran, A. M. Turner, D. P. Arovas, and A. Vishwanath, *Nat. Phys.* **9**, 299 (2013).
- [112] H. Watanabe, H. C. Po, A. Vishwanath, and M. Zaletel, *Proc. Natl. Acad. Sci.* **112**, 14551 (2015).
- [113] Y. Ogata, Y. Tachikawa, and H. Tasaki, *arXiv preprint arXiv:2004.06458* (2020).